Send Orders of Reprints at reprints@benthamscience.org

5062 *Current Medicinal Chemistry,* 2012, *19,* 5062-5087

Tell Me Something I Do Not Know. Multiscale Molecular Modeling of Dendrimer/Dendron Organization and Self-Assembly In Gene Therapy

P. Posocco[1], E. Laurini[1], V. Dal Col[1], D. Marson[1], K. Karatasos[2], M. Fermeglia[1] and S. Pricl*[,1,3]

[1]*Molecular Simulation Engineering (MOSE) Laboratory, Department of Industrial Engineering and Information Technology (DI3), via Valerio 10, 34127 Trieste, Italy;* [2]*Department of Chemical Engineering, University of Thessaloniki, P.O. BOX 420, 54124 Thessaloniki, Greece;* [3]*National Interuniversity Consortium for Material Science and Technology (INSTM), Research Unit MOSE-DI3, University of Trieste*

Abstract: Due to the relative easy synthesis and commercial availability, nanovectors based on dendrimers and dendrons are among the most utilized non-viral vectors for gene transfer. Contextually, recent advances in molecular simulations and computer architectures not only allow for accurate predictions of many structural, energetical, and eventual self-assembly features of these nanocarriers *per se*, but are able to yield vital (and perhaps otherwise unattainable) molecular information about the interactions of these nanovectors with their nucleic acid cargoes. In the present work, we aim at reviewing our own efforts in the field of multiscale molecular modeling of these interesting materials. In particular, our originally developed computational recipes will be presented, and the link between simulations and experiments will be described and discussed in detail. This review is written by computational scientists for experimental scientists, with the specific purpose of illustrating the potentiality of these methodologies and the usefulness of multiscale molecular modeling as an innovative and complementary tool in their current research.

Keywords: Multiscale molecular modeling, dendrimers, dendrons, self-assembly, gene therapy.

THE PLEASURE OF UNPLEASANTNESS

With the conclusion of the human genome-sequencing project, the medical research community has an unparalleled opportunity to understand and cure diseases on a genetic level. However, translating this genomic information into drug therapies is still a major challenge facing researches in the fields – up to the pre-clinical stage - as well as pharmaceutical companies for the later stages of development. Providing support for the concept that drug modulation of a given target is likely to produce a therapeutic response in patients is a key step in this progression from "gene to screen". The main limitations are knowing which gene products are functionally involved in the pathology of a disease (target validation) and the druggability of the gene products by natural and/or synthetic compounds.

Recently, gene therapy, which holds enormous potential for therapeutic intervention of a broad range of genetic diseases, including viral pathologies, gene-related disorders, and cancer, has been recognized as an alternative approach to overcome the drawbacks of "standard" therapies. Gene therapy aims at delivering DNA, RNA, or antisense sequences that alter gene expression within a specific cell population, thereby manipulating cellular processes and responses [1]. Notwithstanding the wide range of nucleic acids therapeutics that are currently emerging as powerful, new drug entries for the treatment of gene-related diseases and for lead validation in the drug discovery process, there are still significant obstacles to be overcome before these types of therapeutics can be exploited in the clinic [2, 3].

Perhaps, foremost among these is the issue of delivery. The *in vivo* use of DNA/siRNA effective against cancer or other genetic maladies hinges on the availability of a delivery vehicle that can be systematically administered to reach the target cells. Moreover, because of sufficient intact, functional genetic material must be delivered into cells to reach an effective intracellular concentration, and to limit potential side effects due to a randomized, general transfection of normal, non-target tissues, it is also crucial to develop means of directing such a delivery vehicle specifically to the target cells [4, 5].

Injected nanoscale drug delivery systems, or *nanovectors*, are ideal candidates to provide breakthrough solutions to the time-honored problem of optimizing therapeutic index for a treatment. Even modest amounts of progress towards this goal have historically engendered substantial benefits across multiple fields of medicine, with the translatability from, for example, a subfield of oncology to a field as distant as the treatment of infectious diseases being granted by the fact that the progresses had a single common denominator in the underlying technological platform [2, 4, 6, 7].

Synthetic nanovector systems have much to offer in this respect. They can be structurally varied, are relatively safe to produce, and are able to carry large and diverse genetic material into cells. Accordingly, studying their biological and physico-chemical properties by structural modification represents an exciting challenge for chemists as this approach constantly provides new and valuable information for the design of more complex and efficient systems [8].

However, any synthetic agent to deliver genetic material specifically will be exposed to biological mechanisms that unavoidably limit its trafficking both outside and inside the cells. In summary, an ideal synthetic vector should tightly compact the foreign nucleic acid, transport it through cellular membranes while ensuring its protection from degradation and allow its recognition and activation by the cell machinery. Of course, the synthesis of a *magic bullet* affording all these skills together remains idealistic; nevertheless, many synthetic vectors have been active enough to justify concentrated research efforts and sometimes, even commercialization. More specifically, nanoparticles based on linear, branched, hyperbranched and dendrimeric polymers constitute an attractive variety of synthetic vectors for cell transfection today see Fig. (**1**).

Dendrimers and dendrons are polymeric vectors made of monomers that emanate radially from a central core [10]. The size of these branched structures is typically of the order of 1-10 nm, but this size can be fine-tuned by varying the dendrimer generation number. In addition to their size, their architecture and chemical constitution (e.g., end groups) can be precisely controlled, a direct function of the step-by-step synthesis involved in dendrimer fabrication [10, 11]. The resulting vehicle is an attractive platform for drug delivery, in light of the presence of a central cavity and channels between dendrons wherein drugs can be entrapped [12]. In addition to drug loading within this void spaces, drug can be grafted onto tailorable functional groups [13]. This affords the possibility of incorporating not only multiple and different drug molecules within the same dendrimer, but also multiple targeting ligands as well [14].

*Address correspondence to this author at the MOSE-DI3, University of Trieste, Via Valerio 10, 34127 Trieste, Italy; Tel: +39-040-5583750; Fax: +39-040-569823;
E-mail: Sabrina.Pricl@di3.units.it

1875-533X/12 $58.00+.00

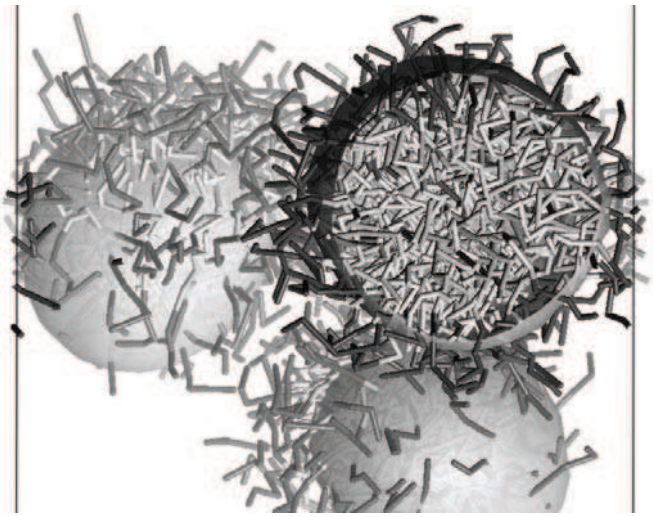

Fig. (1). Three-dimensional model of spherical micellar nanovectors for drug delivery. Adapted from [9], with permission of the RSC.

THE NANOTECHNOLOGY CHALLENGE

We could define nanomedicines as delivery systems in the nanometer size range (preferably 1 to 100 nm) [15] containing encapsulated, dispersed, adsorbed or conjugated drugs and/or imaging agents. Further, when considering nanocarriers, these systems should possess multiple desirable attributes [16]. First, nanoscale drug delivery systems must have the ability to improve the pharmacokinetics and increase the biodistribution of therapeutic agents to target organs, which results in improved efficacy. Second, they should exhibit a preferential accumulation at target sites and lower concentration in healthy tissues, so that the cargo drug toxicity is reduced. Third, nanocarriers must have the desirable advantage in improving solubility of hydrophobic compounds in the aqueous medium to render them suitable for parenteral administration. Fourth, delivery systems must exert a stabilizing effect on a wide variety of therapeutic agents such as small hydrophobic molecules, peptides, and oligonucleotides.

Nanoparticles (NPs) are man-made small objects, with a nanometer characteristic size, that are injected at the systemic level (intravascularly) to execute specific diagnostic and/or therapeutic missions at the biological target site. This could be a tumor mass, an inflamed portion of the vasculature, or any district within the human body where abnormal cells are proliferating. Before reaching the target site, the blood-born NPs must make their way into the circulatory system passing a multitude of barriers that simply tend to sequester, digest and/or expel any foreign object, as the NPs. Additional impediments are of the biological barrier type, which include the reticular endothelial system (RES), constituted by phagocytes, specialized cells lining the liver, spleen, bone marrow, and lymphatic tissues, which recognize external molecules and remove them from the circulation. Moreover, it is important to note that the type and severity of the barrier is disease and patient specific.

However, success in targeting is not just about performance at the target site. There will be for instance loss of drug from the carrier by anticipated release or degradation, loss of the cargo/carrier complex through uptake into non-target sites, or reduced thermodynamic activity of the active principle once it is sequestered by proteins. The system may fail to reach the target in sufficient quantity, and payload release rate and the rate of diffusion of the free drug may be suboptimal to achieve therapeutic effects. It is one thing for a nanocarrier to reach a target tissue but another for its active cargo to be still bound to its vector and not lost en route or, conversely, bound too tightly that it is not released at the site of action. Recirculation of systems clearly provides further opportunity to engage with the target, but also prolongs the lifetime of the carrier in the circulation and, with most systems presently available, this increases the chances of drug leakage and premature drug loss if release is time-dependent, rather than triggered by some mechanism (e.g., pH variation or enzymatic reaction) close to the target.

With such a complex biological scenario, and with the multitude of possibilities chemists have at hand, devising new, efficient and safe nanovectors based only on empirical or semi-rational design has become a tantalizing task. Thus, accurate predictive mathematical or molecular models are fundamental in identifying those properties that can maximize all the structural and physicochemical properties required to an ideal nanocarrier.

(MULTISCALE) MOLECULAR MODELING TO THE RESCUE!

Molecular modeling and engineering is indeed entering a new era, characterized by an unprecedented control over chemical reactions, as well as product molecular architecture, conformations and morphology. It is entering an era of molecular processing and manufacturing in which single-molecule experiments are becoming routine and complex miniature processes are beginning to be commercialized for a number of different applications. These experiments and processes not only benefit from modeling but, in some cases, must be interpreted or implemented through concerted multilevel molecular modeling efforts.

Indeed, molecular modeling of biophysical phenomena at different length and time scales is crucial for identifying the main parameters governing the space-temporal evolution of the system under investigation, for elucidating the role and quantifying their effects and, most importantly, for predicting the evolution of the system prior to running extensive and expensive experiments. Multiscale molecular modeling can indeed be used to design *rational* experiments and to guide or inspire experimentalists. Given the complexity of biology, and the huge biological diversity among apparently similar concepts, computer-assisted multiscale molecular simulations are clearly of fundamental importance for the effective development of reliable predictive tools to be used in the design of new agents in personalized medicine.

The actual computational modeling of biological macromolecules, mainly based on molecular dynamics (MD) simulations, commonly revolves around structure representations in atomic or near-atomic detail, with a classical description of physical interactions. Such models have been quite successful in complementing experimental data with structural, dynamic, and energetic information, but involve substantial computational resources for larger systems, or when long time scales have to be considered. In particular, structure-activity calculation applications, the formation and interaction of supramolecular assemblies, and the prediction of kinetic and transport phenomena will necessarily involve extremely extensive computational resources when using models at atomic details, if they are feasible at all.

Thus, we are also in the need of developing some computational strategy to link the atomic length and time scales of MD to the macroscopic length and time scales (nanometers to micrometers and nanoseconds to microseconds) of the so-called *mesoscale* phase. Only by establishing this connection from nanoscale to mesoscale it is possible to build first principles methods for describing the properties of new materials and systems for biomedical and life science applications, of which RNA/DNA delivery systems are prototypical examples.

However, there are significant challenges in using theory to accurately predict properties for nanoscale materials, especially when (bio)macromolecules are involved. Indeed, despite the tremendous

advances achieved in molecular modeling and simulation techniques, there remains a remarkable uncertainty about how to predict many critical properties related to material final performance. The main problem lies in the fact that most of these properties depend on the interactions and chemistry taking place at the atomic level, involving electronic and atomic descriptions at the level of nanometers in the length scale, and picoseconds in the timescale. Conversely, the pharmaceutical technology designer needs answers from microscopic modeling of components having scales of the order of tens/hundreds of nanometers, and of phenomena taking place in a time range of milliseconds or much larger. Thus, to achieve a dramatic advancement in the skill of designing innovative, highly-performing materials, it is mandatory that we link the atomistic to the microscopic modeling [9, 17].

Molecular modeling and simulation combine methods that cover a range of size scales in order to study material systems. All together, quantum mechanics (QM), molecular mechanics (MM), molecular dynamics (MD) and Monte Carlo (MC) methods, and mesoscale (MS) techniques cover many decades of both length and time scale, and can be applied to arbitrary materials: solids, liquids, interfaces, self-assembling fluids, gas phase molecules and liquid crystals, to name but a few [17]. There are a number of factors, however, which need to be taken care of to ensure that these methods can be applied routinely and successfully. First and foremost of course are the validity and usability of each method on its own, followed by their interoperability in a common and efficient user environment. Of equal importance is the integration of the simulation methods with experiment. Different-scale simulation can be defined as the enabling technology of science and engineering that links phenomena, models, and information between various scales of complex systems. The idea of many-scale modeling is straightforward: one computes information at a smaller (finer) scale and passes it to a model at a larger (coarser) scale by leaving out (i.e., coarse-graining) degrees of freedom The ultimate goal of many-scale modeling is then to predict the macroscopic behavior of a chemico-physical process from first principles, i.e., starting from the quantum scale and passing information into molecular scales and eventually to process scales. The MD level allows predicting the structures and properties for systems much larger in terms of number of atoms than for QM, allowing direct simulations for the properties of many interesting systems. This leads to many relevant and useful results in materials design; however, many critical problems in this field still require time and length scales far too large for practical MD. Hence, the need to model the system at the mesoscale (a scale between the atomistic and the macroscopic) using information retrieved at the atomistic (lower) scale.

This linking through the mesoscale in which the microstructure can be described over a length scale of tens to hundred nanometers is probably the greatest challenge to develop reliable first principles method for practical material design applications. The problem here is that the methods of coarsening the description from atomistic to mesoscale is not as obvious as it is going from electrons to atoms. For example, the strategy for polymers seems quite different from that applicable to metals, which in turn differs from those employed in the case of ceramics or semiconductors. In other words, the coarsening from QM to MD relies on basic principles and can be easily generalized in a method and in a procedure, while the coarsening at higher scales is more system specific for polymer materials due to the larger range of length and time scales that characterize macromolecules.

Scale integration in specific contexts in the field of (bio)macromolecular modeling can be done in different ways. Any *recipe* for passing information from one scale to another (upper) scale is based on the proper definition of many-scale modeling which considers *objects* that are relevant at that particular scale, disregards all degrees of freedom of smaller scales, and summarizes those degrees of freedom by some representative parameters see Fig. (**2**).

As mentioned above, mesoscopic simulations are performed using a coarse-grained molecular model: the particle in a mesoscopic simulation is related to a group of several atoms in the corresponding atomistic simulation. Dissipative Particle Dynamics (DPD) [18] is one of the best established mesoscopic simulation techniques, according to which a set of particles moves following Newton's equation of motion, and interacts dissipatively through simplified force laws. In the DPD model, individual atoms or molecules are not represented directly by the particle, but they are coarse-grained into beads see Fig. (**3**). These beads represent local *fluid packages* able to move independently. DPD thus offers an approach that can be used for modeling physical phenomena occurring at larger time and spatial scales than some other coarse-grained methods as it utilizes a momentum-conserving thermostat and soft repulsive interactions between the beads representing clusters of atoms/molecules.

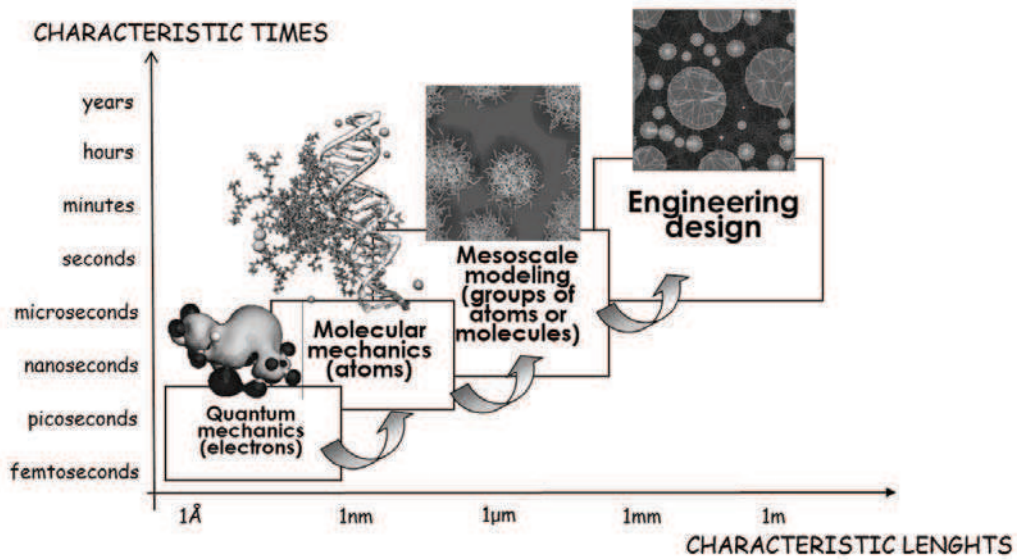

Fig. (2). Our multiscale molecular modeling concept: the information obtained from simulations at a given (lower) characteristic length and time scales is used as an input for the next (upper) scale simulations.

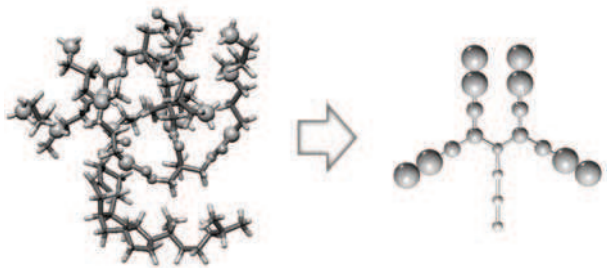

Fig. (3). The coarse-graining concept. Atomistic (left) and coarse-grained DPD (right) representation of a modified dendron as an example.

Specifically, the multiscale modeling strategy developed by our group is based on the systematic elimination of computationally expensive degrees of freedom while retaining implicitly their influence on the remaining degrees freedom in the mesoscopic model. At the coarse-grained (mesoscopic) level, we employed the corresponding most accurate and effective methods/simulation techniques available to investigate physical properties of each system at that level. Accordingly, using the information obtained from atomistic MD simulations we parameterized the coarse-grained (e.g., DPD) models that incorporate all essential physics/phenomena observed at the finer level. The outline of the general strategy of our multiscale modeling approach [17] is as follows:

(1) Extensive explicit solvent atomistic MD calculations (AES-MD) on model compounds and their assembly are carried out. These simulations provide us with dynamic properties/energies that help us to identify important interactions/correlations among the nanocarriers and their cargoes which are to be used *per se* and/or exploited to parameterize the next scale (mesoscale) simulation models.

(2) Using conformational and structural properties obtained from MD simulations at point (1) we parameterize the DPD model in which each nanocarrier and nucleic acid segment are represented as single force centers (beads) and solvent is treated explicitly in the presence of ions and counterions. Langevin dynamics are then conducted using the DPD representation of the system. These simulations are about orders of magnitude computationally less expensive than simulations with the AES-MD model, therefore allowing us to simulate more realistic systems and to significantly extend the accessible time scales. Most importantly, these type of simulations yield topical information of the morphology of the systems under investigation in a length scale (L) range of $1 \leq L \leq 1000$ nm; contemporarily, the time scale can be extended up to seconds, that is, where most of the critical energetical and structural phenomena involved in several aspects of the performance of these systems take place.

(3) Eventually, the equilibrium configurations of the mesoscopic systems obtained at point (3) can be mapped back to the corresponding AES-MD models, and then AES-MD simulations can be used again to obtain more accurate structural/energetical information of the corresponding supramolecular systems (e.g., the case of self-assembled nanovectors, *vide infra*).

Under the multiscale molecular modeling perspective outlined above, the current ambitious aim of our research group is to reach the domain of nucleic acid delivery system engineering by building from fundamental principles of physics and chemistry. Hence, for fundamental predictions to play a direct role in these materials innovation and design, it is mandatory to bridge the micro-macro gap, thus establishing a tight and direct coupling between *in silico* and *in vitro*/*in vivo* experiments.

We are nowadays facing a scenario where modeling for qualitative understanding of physicochemical mechanisms is not sufficient for designing future generations of more powerful, reliable nanodelivery devices; instead, fully predictive modeling capabilities are required. We are among those that firmly believe molecular multiscale modeling can provide a validated technology to tackle such problems on a rational basis.

DO YOU FEEL THE FORCE? (OR COMPUTATIONAL ASPECTS OF DNA/RNA BINDING BY DENDRIMER-BASED NANOVECTORS)

One of the key questions that troubles the mind of every chemist contemplating his/her newly designed or synthesized nanovector for gene therapy undoubtedly is: "Will it interact with and, possibly, bind DNA/RNA?" Indeed, the ability of the nanocarrier to generate a stable complex with its nucleic acid payload is the background postulate for its usefulness. This question finds its experimental answer through the use of many disparate techniques, ranging from the standard Ethidium Bromide (EthBr) displacement fluorescence spectroscopy assay to the more sophisticated and quantitative isothermal titration calorimetry (ITC) or differential scanning calorimetry (DSC). Multiscale molecular simulations, however, not only can yield an answer to this important query, but may offer a reliable molecular rationale to explain the generation, structural, ionic strength, and other chemico-physical properties and mechanisms determining the dependence of the affinity of a given dendrimer/dendron carrier to its nucleic acid cargo, as explained in the examples discussed below.

What a Difference a Core Makes (Or The Role of Nanocarrier Molecular Flexibility in DNA/RNA Binding)

The unique chemistry of dendrimers allows for the controlled degradation through depolymerization or other techniques (e.g., UV irradiation) which may, in turn result in controlled drug release profiles at the site of action. A brilliant practical example of this assertion is the discovery that the DNA transfection efficiency of partially degraded and structurally fractured polyamidoamine (PAMAM) dendrimers is approximately 2 orders of magnitude higher than that of non-degraded molecules [19]. This was originally ascribed to the fact that the presence of defective, shorter branches in the dendrimeric structure results in a less jammed interior molecular organization and a smaller amount of branch backfolding. These properties then endow partially degraded dendrimers with an overall more flexible and open structure compared to their intact counterparts, and hence more accessible for interaction with DNA and RNA via both electrostatic interactions and mutual structural adaptation in space. In addition, a more open and flexible structure could favor a more extensive hydration of the nanovector interior, ultimately increasing the availability of the inner amines for protonation. This, in turn, may result in an enhanced buffering capacity via the so-called *proton sponge effect* [20], finally leading to a more efficient nucleic acid release and, likely, a better transfection efficiency.

Obtaining degraded/fractured dendrimers with precisely reproducible structures is a time-consuming, painstaking practice, resulting in an unsatisfactory, uneconomical, and manpower-wasting process. Elicited by this strong motivation, Peng *et al.* decided to pursue the goal of achieving the same results of superior gene delivery performance from a different perspective: inducing enhanced flexibility in genuine (i.e., non-degraded) PAMAM dendrimers by acting at their very core. Thus, they conceived and synthesized up to generation 7 (G7) PAMAM dendrimers featuring a triethanolamine (TEA) moiety as the dendrimer core [21]. The idea underlying this semi-rational design was that, with TEA as the dendrimer focal point, the branching units would start at a distance of 10 successive bonds away from the central amine whilst, in the case of prototypical NH_3-core based PAMAMs, the branches sprout immediately at the central N-atom of the ammonia core see Fig. (**4**).

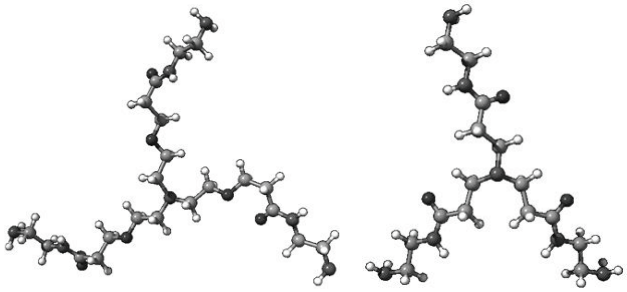

Fig. (4). Chemical structures of the TEA-core (left) and NH_3-core (right) PAMAM dendrimers. For clarity, dendrimers of the first generation (G1) are shown. Color code: carbon, light gray; nitrogen, medium gray; oxygen, dark gray; hydrogen, white.

According to this vision, TEA-core PAMAMs should feature a much more extended and flexible core, and this characteristic should then propagate to the entire molecule, in harmony with the concept that in dendrimers, as a molecular parallelism with higher organisms, beginning with a specific core molecular details are sequentially transcribed and stored to produce interior and ultimately exterior features which are characteristic of that core-based dendrimer family [22]. In other words, TEA-core based dendrimers were expected to have branching units less densely packed and their terminal groups more readily available to interact with DNA/RNA than the NH_3-core molecular counterparts.

Pleasingly, these authors did verify that TEA-core PAMAMs effectively interact with DNA/RNA and efficiently deliver small interference RNAs (siRNAs), and particularly plasmid DNA even *in vivo* [21, 23]. Notwithstanding, they were still wondering whether the excellent performance of their nanovectors was indeed ascribable (at least in part) to their actual enhanced structural flexibility. Thus, together we embarked in a multiscale modeling study to yield a rationale for their experimental observations [23].

At first, using atomistic molecular simulations in explicit solvent (AES-MD), at physiological ionic strength (0.15 M) and pH (7.4) conditions, we studied and compared the interaction of generations 4, 5, and 6 (G4-G6) of TEA-core and NH_3-core dendrimers with DNA. Indeed, the structural diversity induced by the presence of TEA with respect to NH_3 as cores in PAMAM dendrimers clearly emerged from the respective MD simulations. Taking G5 as a proof-of-concept (the same considerations holding for all generations considered), we could unequivocally determine that the TEA-core based PAMAMs are characterized by a more open and flexible conformation featuring voids within its interior while the NH_3-core PAMAMs behave more rigidly, with a more homogeneous distribution of the monomer units and small spaces throughout the entire molecule (see top panels in Fig. (**5**)). Additional insightful structural information on the effect of structural modification on these two dendrimer series stem from MD simulations of their DNA binding (middle panels, Fig. (**5**)). Indeed, the conformation of the TEA-core dendrimers is such that the outer branches can readily move towards the phosphate backbone of DNA during complex formation, and the surface amino groups can arrange themselves via *induced-fit* for optimal binding with the nucleic acid. In contrast, the more rigid and compact structure of the alternative PAMAM molecule prevents it from undergoing a significant conformational rearrangement required by induced-fit; as a consequence, less amine groups are available to self-orient for best DNA binding.

A quantitative evidence of the difference in structural flexibility between these two dendrimer series came from the analysis of the radial density function $\rho(r)$. The bottom panels of Fig. (**5**) show the spatial distribution of the terminal nitrogen atoms of TEA- and NH_3-core dendrimers, both alone and in complex with a short fragment of DNA. From these curves we evince that some backfolding of the terminal amine groups is present in both isolated dendrimers in solution. However, by virtue of its larger core, greater flexibility, and hence higher mobility of its outer arms, the location of maximum terminal group density in the case of the TEA-core dendrimer G5 is shifted towards the molecular periphery with respect to the same generation of the NH_3-core dendrimer (compare the broken-line curves in the bottom panels of Fig. (**5**)). Upon binding to DNA, the differences in the radial density distributions become even more evident, with the density profiles of the primary nitrogen atoms stretching further out towards the periphery in the case of the TEA-core dendrimer G5 due to the electrostatic attraction of the DNA phosphate negative groups. In other words, the charged end-groups of the G5 TEA-core PAMAM dendrimer are able to reposition themselves for optimal binding with the nucleic acid more efficiently than those of the NH_3-core G5 molecule.

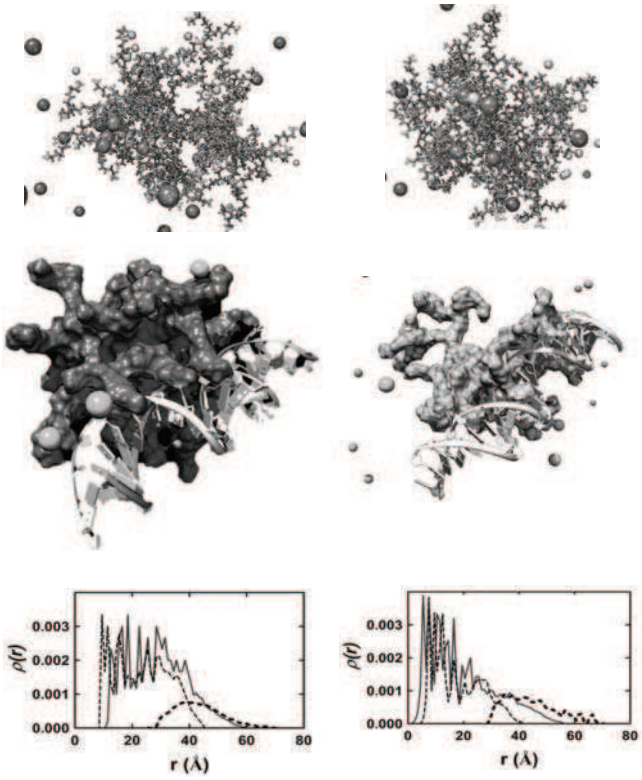

Fig. (5). Top panels: equilibrium MD snapshots of G5 TEA-core (left) and NH_3-core (right) PAMAM dendrimers. The dendrimers are portrayed in mid gray sticks, with the terminal primary amine groups highlighted as light gray sticks-and-balls. Some chlorine (Cl^-) and sodium (Na^+) counterions are shown as dark gray and gray spheres, respectively. Water is not shown for clarity. Middle panels: Equilibrium MD snapshots of the G5 TEA-core (left) and NH_3-core (right) PAMAM dendrimers in complex with a fragment of double-stranded DNA. In this case, the dendrimer molecules are encased in their van der Waals surfaces, while the DNA is depicted as a white ribbon. Bottom panels: radial density distribution $\rho(r)$ of the dendrimer terminal nitrogen atoms in G5 TEA-core (left) and NH_3-core (right) PAMAM dendrimers alone (thin broken lines) and in the complex with DNA (continuous lines). The corresponding distributions of the DNA phosphorus atoms in each DNA/dendrimer complex are shown as thick broken lines. Bottom panels redrawn from [23], with permission of the ACS.

This assertion is supported by the density distribution of the phosphorus atoms in DNA in the corresponding TEA-core G5/DNA complex, showing a good penetration of the DNA fragment within the G5 outer shell. On the other hand, the more compact conformation, higher level of backfolding, and intrinsically higher rigidity of the NH_3-core PAMAM G5 result in a lower den-

sity of terminal amines on the molecular surface, ultimately preventing this molecule from undergoing the substantial conformational readjustment required for optimal DNA binding. This is further confirmed by the corresponding DNA phosphorus density distribution curve, which shows only a partial penetration of the nucleic acid within the molecular structure of the dendrimer with an ammonia core (compare the continuous-line curves in the bottom panels of Fig. (**5**)).

Perhaps most importantly, these marked differences in overall molecular architecture reflect in a manifestly different affinity of these two different PAMAM-based molecules towards DNA or RNA [24]. This can be easily understood looking at (Table **1**), in which the free energy of binding (ΔG_{bind}) between each dendrimer generation and a short fragment of double-stranded (ds) RNA is listed, together with its major components (i.e., the enthalpic contribution ΔH_{bind}, and the entropic term $-T\Delta S_{bind}$, see Supplementary Material for a detailed explanation).

As can be seen in (Table **1**), the free energy ΔG_{bind} is negative for all systems considered, indicating that, at pH = 7.4 and in the presence of 0.15 M NaCl, the association of the nanovectors with their nucleic acid payloads is a thermodynamically favorable and spontaneous process. However, for each dendrimer generation the TEA-core PAMAMs show a superior affinity for the ds-RNA sequence (i.e., ΔG_{bind} more negative) with respect to their NH_3-core counterparts. As somewhat expected, the thermodynamic quantity governing the binding process in both cases is the enthalpy variation, which is also large and negative, and, hence, favors the binding between the nucleic acid and its vector. On the other hand, the entropy variations always afford an unfavorable contribution to binding. Actually, this is an anticipated result, as both molecules lose degrees of freedom upon complex formation with respect to their isolated states in solution.

The last three columns in (Table **1**) show the values of ΔG_{bind}, ΔH_{bind} and $-T\Delta S_{bind}$ normalized by the number of charges N present on each molecule at pH = 7.4 [24]. This normalization procedure is necessary in order to compare the affinity of the different dendrimer generations towards the ds-RNA. Considering these normalized values, from (Table **1**) we not only understand that the affinity of the TEA-core PAMAMs for the nucleic acid is still ranked higher than that of the NH_3-core PAMAMs at all generations but, in both cases, there is a notable increase in binding strength in passing from generation 4 to generation 5, substantially ascribable to an enhanced favorable enthalpic component. This aspect may account for the better binding and, hence, better properties as nanocarriers of the higher dendrimer generations, in accordance with the experimental evidences.

At the same time, the entropy contributions are seen to be lower (i.e., less unfavorable) in the case of TEA-core molecules. This lower value of $-T\Delta S_{bind}$ can once again be connected to a greater conformational change of the dendrimer (allowed by its high flexibility due to the large core) in order to enwrap the ds-RNA, followed by an enhanced productive bending of the nucleic acid for all generations in this dendrimer family.

Thus, atomistic molecular simulations in an explicit solvent and in the presence of the appropriate ionic strength and pH conditions were able not only to answer "yes, it binds DNA/RNA!" but also to offer a molecular-based reason to support the validity of the semi-rational design based on the postulated "larger core = greater flexibility = better nucleic acid binding" hypothesis.

Sweet and Sour (Or Effect of pH in Binding the Nucleic Acids)

A plethora of experimental studies of nucleic acids involving dendrimers as carriers established that high (G4 and up) generation molecules are good candidates for gene delivery purposes since, beyond their capacity to tightly grab and compact DNA/RNA, due to their moderate size they behave as soft deformable particles rather than compact, hard spheres, thus offering a better control upon the response of their conformational properties to changes in the local environment [25].

This concept can be unequivocally confirmed resorting again to AES-MD simulations, and in particular by analyzing the behavior of the dendrimer radius of gyration R_g at different values of the solution pH [24]. It is important to recall here the mean-square radius of gyration R_g can be defined as $R_g = (1/M_W)\left\langle\left[\sum_{i=1}^{N} m_i|r_i - R|^2\right]\right\rangle$, where R is the center of mass of the dendrimer, r_i and m_i are the position and mass of the i^{th} atom, and M_w refers in this case to the total mass of the dendrimer. In other words, the value of R_g represents the average spatial distribution of all dendrimer atoms from a given point in space which, according to the above equation, coincides with the dendrimer center of mass.

Let us then consider the R_g curves shown in the left panel of Fig. (**6**) for G4-G6 TEA-core and NH_3-core PAMAMs in complex with a 19 base-pairs (bps) ds-RNA, and focus on G4 as a proof-of-concept: when the pH value drops below 7.4, an appreciable increase in the dendrimer average radius of gyration can be unmistakably observed. If we then expand the pH range to two (physiologically irrelevant but chemically interesting) extreme values of the acidity scale, i.e. 12 and 4, the estimated R_g overall increase on going from pH = 12 to pH = 4 amounts to nearly 30%. This tendency to swelling is exhibited by all dendrimer generations of both

Table 1. Values of the Free Energy of Binding ΔG_{bind} and its Principal Components Involved in G4-G6 TEA-Core and NH_3-Core PAMAMs Binding to RNA at pH 7.4. The Last Three Columns Show the Same Values Normalized by the Total Number of Dendrimer Charged Amine Groups N at pH 7.4. All Values are in kcal/mol. Adapted from [24], With Permission of John Wiley & Son

TEA-Core PAMAMs						
G	**ΔH_{bind}**	**$-T\Delta S_{bind}$**	**ΔG_{bind}**	**ΔH_{bind}/N**	**$-T\Delta S_{bind}$/N**	**ΔG_{bind}/N**
4	-432 ± 11	99 ± 10	-333 ± 15	-9.82	2.25	-7.57
5	-788 ± 13	133 ± 11	-655 ± 17	-17.9	3.02	-14.9
6	-902 ± 13	156 ± 10	-746 ± 16	-20.5	3.55	-17.0
NH_3-core PAMAMs						
G	**ΔH_{bind}**	**$-T\Delta S_{bind}$**	**ΔG_{bind}**	**ΔH_{bind}/N**	**$-T\Delta S_{bind}$/N**	**ΔG_{bind}/N**
4	-353 ± 16	152 ± 12	-201 ± 20	-8.02	3.45	-4.57
5	-702 ± 14	195 ± 10	-507 ± 17	-16.0	4.43	-11.5
6	-829 ± 13	210 ± 10	-619 ± 16	-18.8	4.77	-14.1

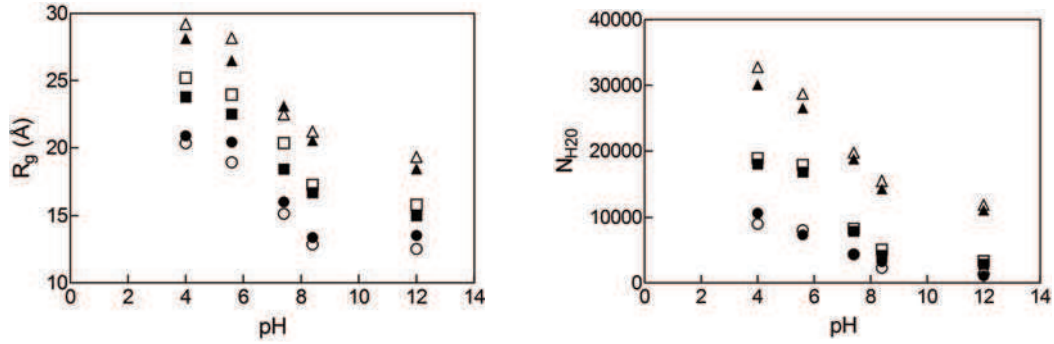

Fig. (6). (Left) Radius of gyration R_g as a function of the solution pH for G4-G6 TEA-core (open symbols) and NH_3-core (filled symbols) PAMAMs in complex with a small fragment of ds-RNA. (Right) Number of water molecules in the G4-G6 TEA-core and NH_3-core PAMAM dendrimer interiors as a function of the solution pH. Symbol legend: circles, G4; squares, G5, triangles, G6. Error bars are smaller than symbols. From [24], with permission of John Wiley & Son.

PAMAM series, as somewhat expected. Yet, each dendrimer inherent chemical and structural characteristics (e.g., number of protonable amines, flexibility, …) ultimately reflect in different macroscopic properties: for instance, the more flexible and open-structure TEA-core PAMAMs are more prone to swelling at lower pH than their corresponding NH_3-core counterparts.

As anticipated above, the systematic behavior exhibited by G4 in the entire range of pH is observed also for the successive generations, although the degree of swelling is less pronounced moving to higher generations (G5 and G6), due to the unavoidable, progressively increased intricacy of the dendrimer interior. Importantly, however, the structural characteristics propagated by different cores throughout the entire dendrimeric scaffolds endow the molecules with different swelling capacities. Thus, the TEA-core PAMAMs characterized by the presence of an enlarged core and a more open conformation with void spaces is more inclined to swelling at pH < 7.4 than the more rigid and dense NH_3-core series.

From a structure-activity relationship (SAR) standpoint, the enhanced swelling capacities of the TEA-core dendrimers at low pH values may result in a higher buffering capacity which, in turn, can be beneficial to endosomal escape of the nucleic acid cargo via the proton sponge effect [20]. At the cellular level, in fact, inadequate cytosolic access is one major challenge that must be overcome if nanovector/DNA(RNA) systems are to become effective *in vivo* therapeutics. The increased swelling and, possibly, the increased proton sponge effect of more flexible and open structure dendrimers such as the TEA-core PAMAMs undoubtedly concur to enhance the capacity of these nanovectors and their cargoes to enter the endosome, adsorb protons, swell and cause an influx of negative (e.g., Cl^-) counterions which, in turn, creates an osmotic effect ultimately leading to water uptake. This escalation of events are purported to cause endosome membrane destabilization and rupture, with subsequent release of the nanodelivery complex in the cellular cytosol. Thus, should the proton sponge effect be the operative mechanism underlying endosome escape of the nanovector and release of it payload, then flexibility, softness, and conformational freedom are all key molecular parameters in a dendrimer-based nanocarrier.

The Yin and Yang of a Dendrimer Core (Or Analysis of the Proton Sponge Effect)

For deeper insight on how the conformational rearrangements triggered by changes in pH affect the complexation characteristics between a given dendrimer-based nanovector and its nucleic acid cargo, we monitored the density distribution of a ds-RNA fragment with respect to the center of mass of its dendrimer vector in the corresponding TEA-core and NH_3-core dendrimer complexes, as shown in Fig. (**7**).

A cursory glance at Fig. (**7**) immediately reveals that as the pH level drops, the RNA density distribution become broader and progressively shifts towards the dendrimer interior. Interestingly, for the NH_3-core PAMAM G4, at both physiologically relevant pH values 7.4 and 5.6 – but particularly at pH 7.4 - the ds-RNA seems to be able to penetrate somewhat deeper within the dendrimeric branches than in the case of its TEA-core counterpart. At the lowest pH value, no sensible differences can be discerned in the RNA density profiles but, for the poorly protonated or the fully unprotonated states, a reverse situation can be envisaged, in which the RNA is kept closer to the dendrimer surface in the case of the TEA-core PAMAM with respect to the NH_3-core case.

The main features of the distributions corresponding to the two examined dendrimer topologies share common characteristics. This is also reflected in the behavior of the average distance of the centers of mass between the RNA cargo and its dendritic nanovector in each complex, as is illustrated in Fig. (**8**) for the TEA- and NH_3-core G4 PAMAMs as an example.

From very low values of the pH up to 7.4, the center of mass of the ds-RNA approaches that of the dendrimers at distances near to, or even closer than, the radius of gyration of the nanocarrier. In this respect, the protonation state being equal, the two systems bearing different cores behave in a similar manner within the simulation error margins. Importantly, higher generation molecules follow an utterly analogous trend for these structural features as a function of the environmental pH.

Although no conclusions regarding the association mechanisms between these two families of dendritic nanovectors and their RNA/DNA payloads can be drawn at this stage, it appears that a threshold level of protonation does exist (i.e., 7.4) below which the average separation between the two molecular entities i) is unaffected by the differences in dendritic topology and ii) remains close to the dendrimer radius of gyration R_g.

This *in silico* discovery may have profound implications in the rational design of dendrimer-based nanovectors in gene therapy. Indeed, if on one side concerted evidences point to great molecular flexibility and a substantial presence of voids and cavities within the nanocarrier structure as key parameters for fostering delivery and transfection activity via enhanced swelling and, hence, proton sponge effect (or similar mechanisms), on the other side the same molecular characteristics concomitantly augment the affinity of the nanovectors for their nucleic acid cargoes - particularly at lisosomal pH value – which may ultimately result in a less efficient in-cell payload delivery and, ultimately, reduced therapeutic activity.

The above evidences, discussions and reasoning are further supported by quantitative estimations of the "intensity" of binding (ΔG_{bind}) between the nucleic acid and their nanocarriers at 5.6, as

shown in (Table **2**), especially if compared to those pertaining to pH = 7.4 (compare values in Tables **1** and **2**).

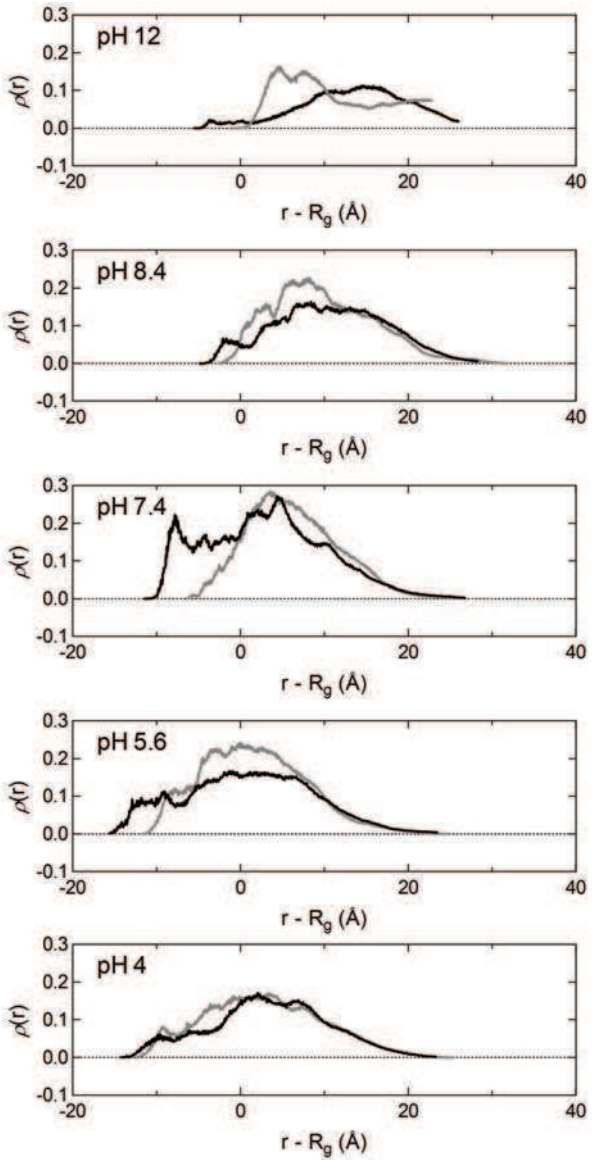

Fig. (7). Radial density distribution of the ds-RNA fragment with respect to the center of mass of the dendrimer in the corresponding TEA-core (gray) and NH_3-core (black) G4 dendrimer/RNA complexes. Note that, in the x-asis, the distance r is corrected for the dendrimer own R_g value; in other words, the 0 value of the x-axis indicates a distance corresponding to R_g. Adapted from [24], with permission of John Wiley & Son.

First of all, contrarily to what observed at pH = 7.4, at this acidic pH the enthalpy of binding ΔH_{bind} for both TEA-core and NH_3-core dendrimer/RNA complexes increases almost linearly with increasing dendrimer generation. But, more significantly, the values of the normalized free energy of binding are smaller (i.e., less negative) in this case. This means that, notwithstanding the increased number of charges present on the nanovectors at pH = 5.6, the augmented swelling and, consequently, the increased dendrimer dimensions reflect in a surface charge distribution less effective in binding the nucleic acid which, in turn, might be beneficial for the subsequent cargo discharge during/after endosomal escape.

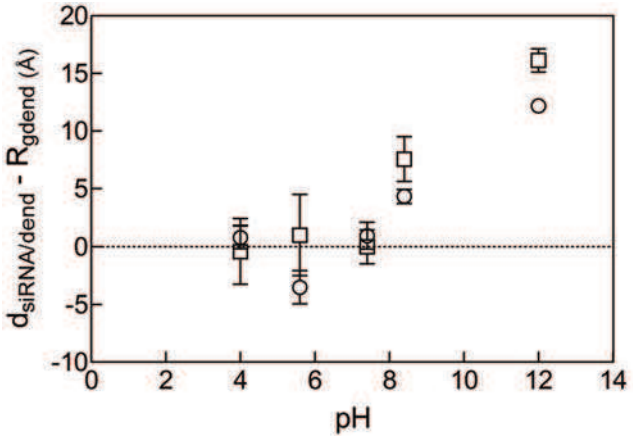

Fig. (8). Average distance between the centers of mass of the G4 dendrimer and a ds-RNA segment as a function of the pH in the corresponding complexes. Symbol legend: TEA-core PAMAM, circles; NH_3-core PAMAM, squares. From [24], with permission of John Wiley & Son.

Waterworld (Or Influence of Water in DNA/RNA Binding by Dendrimer-Based Nanovectors)

As discussed above, soft colloids and macromolecules with flexible structures and void pervading their entire complex molecular structure are necessarily hydrated not only in their outer shell. Indeed, ions and water can penetrate along the tortuous pathways of holes and channels of the macromolecular entity, eventually reaching down to the inner core. In harmony with the foregoing discussion of the propensity of dendrimers to swell in water (particularly at low pH) and of the role of the conformational and chemicophysical features of a given dendrimers in the corresponding ability to adapt to an environmental change, we can expect more flexible dendrimers (e.g., TEA-core PAMAMs) to be more hydrated than dendrimers characterized by a more rigid scaffold (e.g., NH_3-core series). This is indeed the case, as quantified in the right panel of Fig. (**6**): the greater swelling capacity induced by a more flexible structure (TEA-core) favors the penetration of a higher amount of water molecules within the dendrimer interior, particularly at high generations and low pH (both fundamental parameters for efficient delivery), the number of intra-dendrimer water molecules growing almost linearly with pH and paralleling the trend of the corresponding R_g.

Upon binding of the dendrimer to the nucleic acid, water plays even more determining roles. First, it creates a bridge between the carrier and the DNA/RNA, by maintaining an hydration layer and ensuring the instauration of a hydrogen bond network between the carrier and the nucleic acid, critical to their complex formation and stability see Fig. (**9**, top).

More important, perhaps, is the role of overall solubilization. Water and the solution navigating salts must pervade the entire system to guarantee uniform hydration and dispersion of the loaded nanoparticles, avoiding their aggregation and collapse. Mesoscale simulations offer the possibility to predict and study this type of behavior; in fact, a typical result of a mesoscale simulation is the morphology and the structure of matter at nanoscale level at the desired environmental conditions [23]. Let us then consider the images portrayed in the middle panels of Fig. (**9**), where the nanoscale morphologies of the DNA/G6 complexes of TEA-core and NH_3-core dendrimers are compared. As can be seen, in the case of the TEA-core the dendrimers are able to complex the DNA strands efficiently and homogeneously. On the contrary, for NH_3-

Table 2. Values of the Free Energy of Binding ΔG_{bind} and its Principal Components (ΔH_{bind} and $-T\Delta S_{bind}$) Involved in G4-G6 TEA-Core and NH_3-Core PAMAMs Binding to RNA at pH 5.6. The Last Three Columns Show the Same Values Normalized by the Total Number of Dendrimer Charged Amine Groups N at pH 5.6. All Values are in kcal/mol. Adapted from [24], With Permission of John Wiley & Son

TEA-Core PAMAMs						
G	**ΔH_{bind}**	**$-T\Delta S_{bind}$**	**ΔG_{bind}**	**$\Delta H_{bind}/N$**	**$-T\Delta S_{bind}/N$**	**$\Delta G_{bind}/N$**
4	-507 ± 12	92 ± 9	-415 ± 15	-6.42	1.16	-5.25
5	-815 ± 11	133 ± 11	-682 ± 16	-10.3	1.68	-8.63
6	-1299 ± 14	168 ± 10	-1131 ± 17	-16.4	2.13	-14.3
NH_3-core PAMAMs						
G	**ΔH_{bind}**	**$-T\Delta S_{bind}$**	**ΔG_{bind}**	**$\Delta H_{bind}/N$**	**$-T\Delta S_{bind}/N$**	**$\Delta G_{bind}/N$**
4	-398 ± 12	136 ± 9	-262 ± 15	-5.04	1.72	-3.32
5	-732 ± 12	158 ± 10	-574 ± 16	-9.27	2.00	-7.27
6	-1136 ± 15	183 ± 12	-953 ± 19	-14.4	2.32	-12.1

core G6 some chains are less well enwrapped in the systems, and DNA bundles are still present at the nanoscopic level.

The water density maps at the mesoscopic level not only support the lower-scale (i.e., atomistic MD) results discussed above of a higher degree of hydration but also confirm the more uniform water molecule distribution within the nucleic acid/TEA-core dendrimer with respect to the NH_3-core PAMAM.

The Great Zot! (Or Electrostatic Interactions in Nucleic Acid Complexation by Dendrimers)

Undoubtedly, the most extensively studied dendrimers for nucleic acid delivery are PAMAM dendrimers, which bear primary amines at the dendrimer surface and tertiary amines at the branching units inside. Positively charged at physiological pH (7.4), these primary amines yield a high charge density at the dendrimer periphery which, as can be intuitively envisaged based on elementary chemistry and physics concepts, is the main responsible for electrostatic condensation with nucleic acid (*vide infra*) and binding to the cell surface [26, 27]. On the other hand, it has been demonstrated that, despite the structural similarity between RNA and DNA with negatively charged anionic phosphodiester backbones, electrostatic interactions of DNA/RNA with a cationic polymeric agent bear distinctly different characteristics [28]. On these accounts, we calculated the overall charge distributions of TEA-core and NH_3-core dendrimers in complex with a nucleic acid fragment complexes as a function of the distance from the center of mass of the dendritic molecule [24].

The left panel of Fig. (**10**) depicts the aforementioned effective charge distributions for the G4 systems at the different pH values examined, as an example. Following the changes as the dendrimer protonation degree increases (i.e., shifting from a basic to an acidic environment), we observe the development of a charge modulation pattern. While close to the dendrimer center of mass the overall charge fluctuates around zero, an effective positive excess charge develops at intermediate distances, followed by a negative effective charge located at the dendrimer periphery. Within the statistical accuracy, this behavior characterizes all systems of both TEA- and NH_3-core series.

The negative excess charge might be related to the presence of the nucleic acid polyanion close to the dendrimer surface, since the negative area of the profiles shifts toward longer distances from the dendrimer center of mass, in line with the expansion of the dendrimer dimensions upon increasing of its protonation state (see left panel in Fig. (**6**)). This evidence is quite important as it confirms that, notwithstanding the fact that the overall effective charge of the complex is almost zero (i.e., the negative parts of the curves are counterbalanced by its positive parts), the complexes develop a persistent polar character. Moreover, the appearance of the polar character of the complexes can already be observed at pH values close to physiological levels, implying that this mechanism may well affect the behavior of such complexes in *in vitro* and *in vivo* experiments conducted under physiological pH conditions.

Focusing attention on the two pH values of physiological relevance (7.4 and 5.6), in the middle and right panels of Fig. (**10**) we show the charge distribution curves for nucleic acid complexed by dendrimers of generation 5 and 6. Importantly, the main feature characterizing the charge behavior of the G4/RNA complexes discussed above — that is the development of areas of excess positive and negative charge — is still present in these cases; however, significant differences must be highlighted as well. Aside from the fact that charge fluctuations within the dendritic structure seem to increase with increasing dendrimer generation, as generation grows the electrically neutral part of the complex appears to extend at distances comparable to the radius of gyration of the dendrimer. In other words, for high dendrimer generation assemblies the polar area of the complex is mostly located close to the dendrimer surface rather than extending well within the dendrimer interior. This might be one of the aspects of the complex rationale underlying the enhanced DNA/RNA binding and delivery capacity of these bigger nanovectors with respect to the smaller counterparts.

The Dark Side of the Moon (Or Looking at RNA/DNA Complexation from the Nucleic Acid Perspective)

When considering the development of a new, efficient dendrimer-based nanovector for gene therapy, it is more customary to consider the structural and chemico-physical characteristics of the nanovector, and try to optimize them for gene uptake and delivery. In the case of small fragments of nucleic acid, and specifically siRNAs, however, it might be worth considering the gene side as well, and the possibilities this offers in enhancing the interaction of a nanocarrier with its own cargo. Indeed, quite recently it has been shown that siRNAs with short, complementary A_n/T_n overhangs (with n = 5-8, see left panel in Fig. (**11**)), aka known as *sticky* siRNA, could dramatically improve gene silencing efficiency when delivered using the standard poly(ethylene imine) (PEI) as the delivery agent [29]. The purported mechanism underlying these great performance is that the presence of the complementary A_n/T_n over-

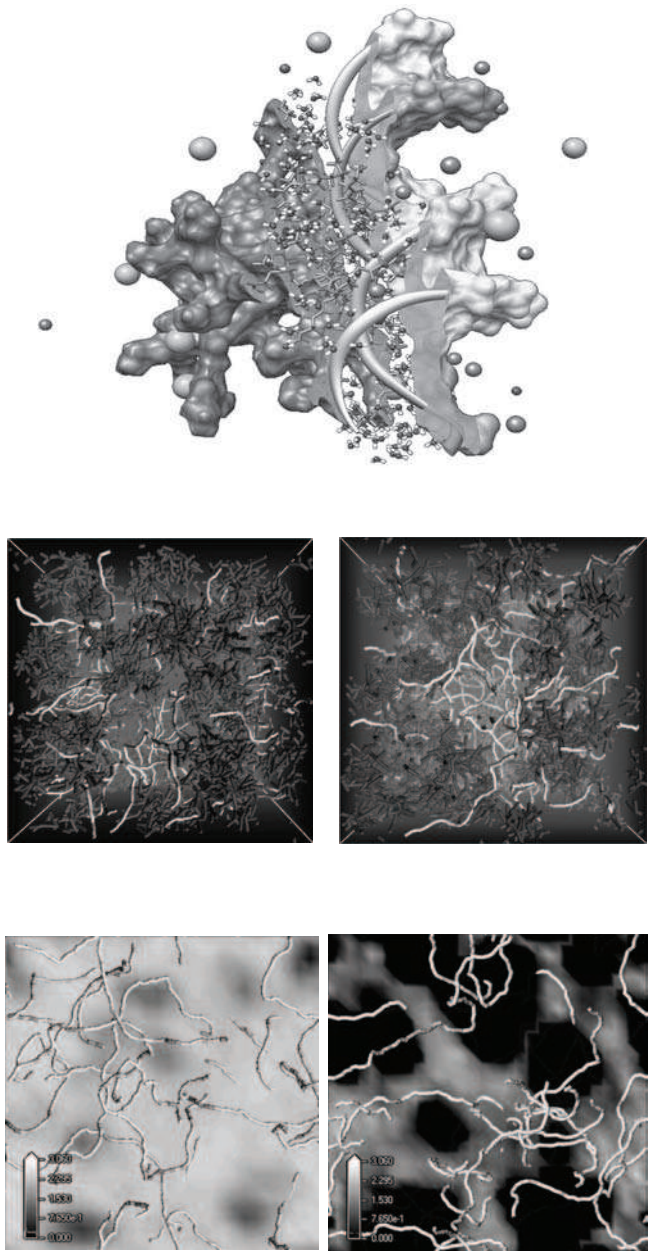

Fig. (9). (Top) Equilibrated molecular dynamics snapshot of G4 TEA-dendrimer in complex with a fragment of ds-DNA, highlighting the water molecules at the interface between the nucleic acid and the dendrimer. The interfacial water molecules are portrayed in dark-gray (oxygen) and white (hydrogen) sticks. All other graphical setting as in Fig. (**5**). (Middle panels) Mesoscale morphologies of the assembled systems between TEA-core dendrimers G6 and DNA (left) and NH_3-core dendrimers G6 and DNA (right). The dendrimers are represented as dark and medium dark sticks while the DNA is shown as white sticks. Water is portrayed as a light gray field. The lower panels highlight the different DNA chains and water molecules distribution within the architectures of the TEA-core (left) and NH_3-core (right) DNA/G6 nanoscopic assemblies. In this case, water is represented as a grayscale density field: according to the scale reported in the lower left corners of the panels, low density values are black, while high density values are white. Middle and bottom panels adapted from [23], with permission of the ACS.

hangs on the siRNA fragment can self-assemble into "gene-like" long double-stranded RNA (see right panel of Fig. (**11**)), and these structure ultimately allow for their successful delivery into cells by PEI with a process utterly similar to that presiding over plasmid DNA delivery.

Given these premises, since the large-scale synthesis of good quality, high generation dendrimers is particularly challenging, we reasoned that, resorting to sticky siRNAs, it could be possible to achieve the same gene efficiency by exploiting lower generation dendrimers as nanovectors.

Indeed, we verified that TEA-core PAMAM dendrimers of generation 5 are able to deliver sticky siRNAs bearing complementary $A_{5(7)}/T_{5(7)}$ 3'overhangs efficiently to a prostate cancer model both *in vitro* and, most notably, *in vivo*, and produce potent gene silencing of the heat shock protein 27, leading to a notable anticancer effect [30].

We further checked whether, in addition to the hypothesized formation of gene-like longer double strand RNA molecules, the two complementary A_n/T_n (n = 5 or 7) overhangs of the sticky siRNAs might also behave as a sort of protruding molecular arms, allowing the siRNA molecule to enwrap the spherical, low generation dendrimers with higher binding affinity compared with a conventional siRNA which has two short T_2/T_2 overhangs. Therefore, we studied the complex formation of G5 with different siRNA molecules (conventional siRNA with T_2/T_2 overhangs, and sticky siRNAs with either A_5/T_5 or A_7/T_7 overhangs) by atomistic MD techniques see Fig. (**12**). The structural differences between these complexes are blindingly obvious: both longer overhangs (A_5/T_5 and A_7/T_7) significantly enhance binding of the sticky siRNAs to the G5 dendrimer by forming more compact complexes. In both these cases (middle and right panels in Fig. (**12**)), not only the unmatched nucleotide sequences act as anchoring points for the siRNA onto the dendrimer surface, but also the double-stranded portion of the siRNA better adapts its overall conformation for a more efficient nucleic acid/nanovector interaction. On the contrary, the presence of the short T_2/T_2 overhangs does not result in a substantial improvement of dendrimer binding by the relevant siRNA (left panel in Fig. (**12**)).

All these pictorial evidences can quantitatively substantiated by the corresponding values of the free energy of binding, ΔG_{bind}, between each sticky siRNA and the G5 dendrimer, as estimated by the MM/PBSA analysis (see Supplementary Material for more information). Indeed, the ΔG_{bind} values obtained for G5 and the sticky siRNAs with A_5/T_5 or A_7/T_7 overhangs are lower (i.e., more negative) than that calculated for G5 and the conventional siRNA with T_2/T_2 overhangs (Table **3**), which indicates that the binding affinity of G5 for sticky siRNAs is higher than that of G5 for conventional siRNA. Based on these results, we hypothesized that, in addition to the possible formation of gene-like longer double strand RNA molecules, stronger binding to dendrimer of sticky siRNAs over conventional siRNAs might also contribute to the enhanced delivery activity of G5.

MULTIVALENCY IN ACTION!

Multivalent systems are widely found in nature, and especially in biology: adhesion of viruses or bacteria to cells' surface, cell to cell adhesion, and cell to polyvalent molecule interactions. A good example of multivalency resides in the defense process of the immune system involving bacteria, antibodies, and macrophages. Antibodies have the ability to recognize *non-self* entities, such as bacteria, upon polyvalent binding with antigens, or other proteins, located at their surface. It is noteworthy that weak ligand-receptor interactions can be made much stronger simply by the simultaneous bonding of these ligands to these multiple receptors.

High-affinity molecular recognition of biomolecular targets is of crucial importance in the development of synthetic systems ca-

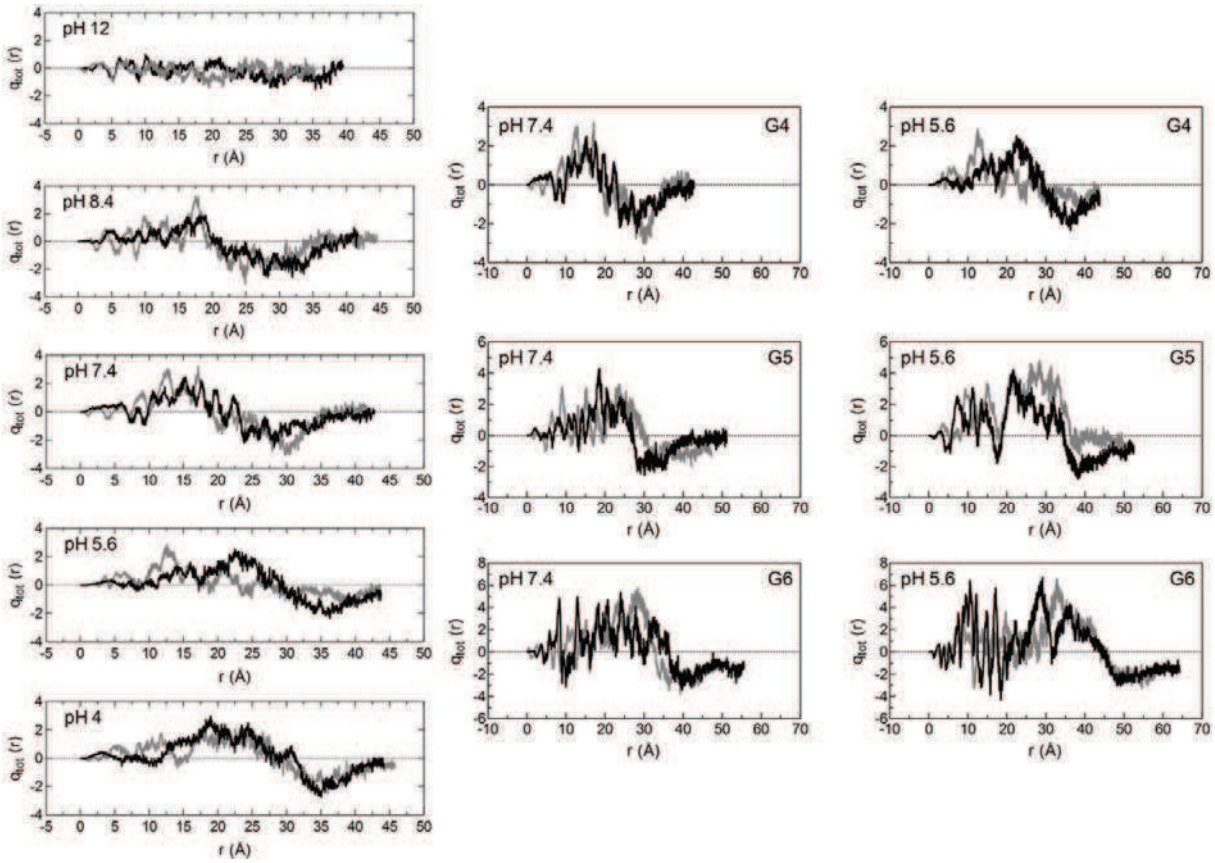

Fig. (10). (Left panel) Effective charge distributions with respect to the center of mass of the dendrimer for the complex of a ds-RNA fragment and TEA-core (gray) and NH_3-core (black) G4 PAMAM dendrimers at different pH values. (Right panel) Effective charge distribution with respect to the center of mass of the dendrimer for the complexes of the same ds-RNA and TEA-core (gray) and NH_3-core (black) G5 and G6 PAMAMs at two physiologically relevant pH values. Adapted from [24], with permission of John Wiley & Son.

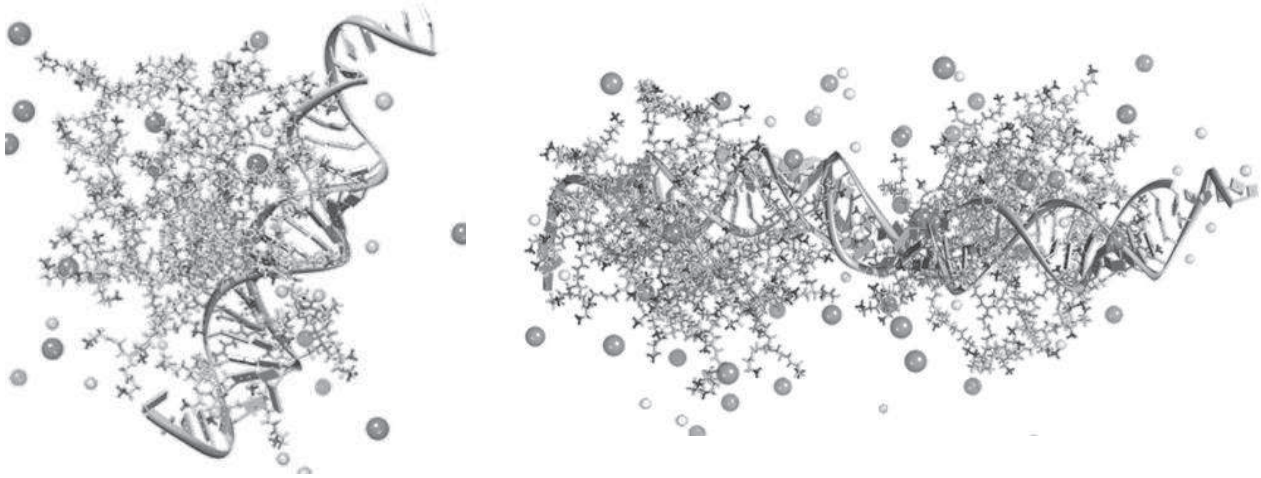

Fig. (11). (Left) Equilibrated molecular dynamics snapshot of the G5 TEA-core dendrimer in complex with a 20 base pairs sticky siRNA carrying complementary A_5/T_5 overhangs at the 3' ends. (Right) Equilibrated molecular dynamics snapshot of the macro-complex resulting from the self-assembly of the siRNA complementary sticky hands. The dendrimers are shown as grey sticks with terminal groups highlighted in black. The siRNA is portrayed as a ribbon, with the bases shown as slabs. Cl^- and Na^+ counterions are painted as gray and white spheres.

pable of intervening in biological pathways; multivalent recognition is a key principle in enhancing binding strength and hence developing systems with potential biomedical applications [31]. Experimental studies and mathematical models have demonstrated that once the first ligand in a multivalent array has bound to the target, the binding of a second ligand is usually a cooperative, entropically less disfavored process, with a local concentration effect also enhancing binding.

Dendrimers and dendrons are inherent multivalent ligands that can present multiple recognition elements from a central scaffold. The scaffold plays a crucial role because it molds the final architecture in term of shape, orientation of recognition elements, flexibil-

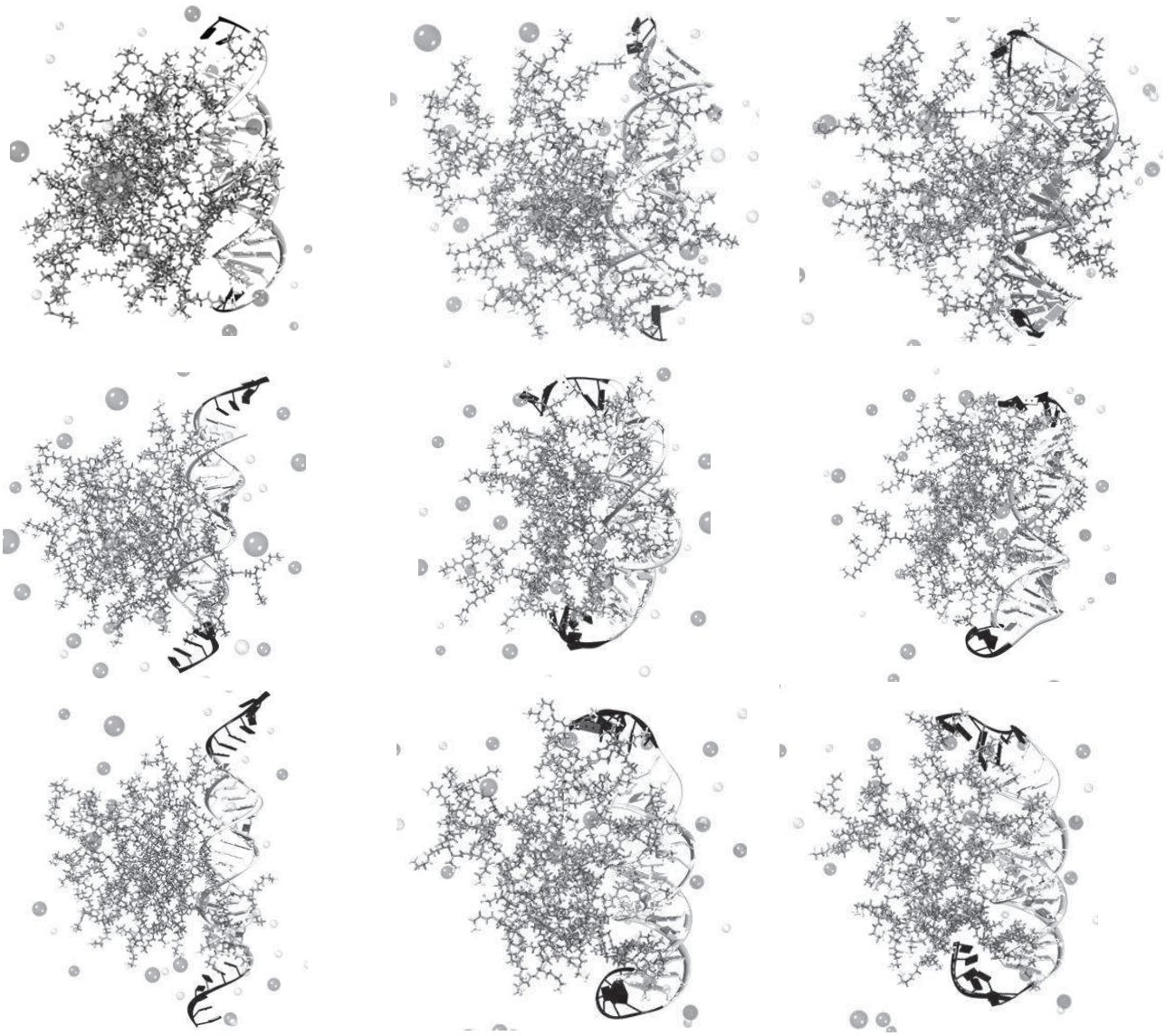

Fig. (12). Equilibrated molecular dynamics snapshots of the G5 TEA-core dendrimer in complex with siRNA molecules bearing T_2/T_2 (top panel), A_5/T_5 (middle panel), and A_7/T_7 overhangs at pH 7.4 and in the presence of 0.15 M NaCl. MD frames are taken after 10 ns (left column), 50 ns (middle column), and 100 ns (right column). Graphical scheme as in Fig. (**11**). Adapted from [30], with permission of the ACS.

Table 3. Free Energy of Binding Between a TEA-Core PAMAM Dendrimer of Generation 5 (G5) and a siRNA with T_2/T_2, A_5/T_5, and A_7/T_7 Overhangs (Conventional siRNA and Sticky siRNAs), Respectively. ΔH_{bind}, $-T\Delta S_{bind}$, and ΔG_{bind} Represent the Enthalpy, Entropy, and Free Energy of Binding Between the Dendrimer and the Different siRNAs. $\Delta H_{bind}/N$, $-T\Delta S_{bind}/N$, and $\Delta G_{bind}/N$ are the Corresponding Normalized Thermodynamic Quantities Per Charge on the siRNA (N). From [30] With Permission of the ACS

System	N	ΔH_{bind} (kcal/mol)	$-T\Delta S_{bind}$ (kcal/mol)	ΔG_{bind} (kcal/mol)	$\Delta H_{bind}/N$ (kcal/mol)	$-T\Delta S_{bind}/N$ (kcal/mol)	$\Delta G_{bind}/N$ (kcal/mol)
G_5/siRNA (T_2/T_2 overhangs)	44	-571.1 ± 2.6	254.3 ± 4.3	-316.8 ± 5.0	-13.0± 0.1	5.8± 0.1	-7.2± 0.1
G_5/sticky siRNA (A_5/T_5 overhangs)	50	-637.40 ± 2.8	250.0 ± 4.1	-387.4 ± 5.0	-12.7± 0.1	5.0± 0.1	-7.7± 0.1
G_5/sticky siRNA (A_7/T_7 overhangs)	54	-690.2 ± 4.7	267.3 ± 5.3	-422.9 ± 7.1	-12.8± 0.1	5.0± 0.1	-7.8± 0.1

ity, size and valency. When the multiple surface groups are ligands, the dendritic scaffolding can be considered to act as a kind of nanoscaffolding, organizing the ligand array. As such, dendritic systems have been widely exploited for their potential applications in multivalent biological recognition [32, 33].

It Takes (More Than) Two to Tango: Dendron Self-Assembly in Gene Delivery

Self-assembly is an incredibly powerful concept in modern molecular science. The ability of carefully designed building blocks to spontaneously assemble into complex nanostructures underpins developments in a wide range of technologies, from materials science to molecular biology [34]. Self-assembly is a supramolecular approach which relies on complementary noncovalent interactions, such as electrostatic and van der Waals forces, hydrogen bonds, coordination interactions and solvophobic effects [35]. In self-assembled structures, these temporal intermolecular forces connect to the molecular scale building blocks in a reversible, controllable, and specific way. Of particular value are the possibilities offered by self-assembly to generate nanoscale complexity with relatively little synthetic input. Furthermore, the ability of self-assembled superstructures to behave as more than the sum of their individual parts, and exhibit completely new types of behavior, is of special interest and appealing in (bio)nanotechnology.

Dendrimer chemistry is another key area of nanoscale science, since dendritic molecules can be considered as unique nanoscale toolkits. Self-assembly can offer an alternative, attractive option to labor-intensive dendrimer synthesis by which dendritic building blocks – many of which can be relatively small and, hence, synthetically easily accessible – can be simply assembled into much more sophisticated architectures [36].

There are a number of different ways in which dendrimers or dendrons can be assembled in solution; perhaps the most efficient approach is the one that gives rise to well-defined (i.e., monodisperse) assemblies of dendritic building blocks. The supermolecular structures generated using this approach are generally based on well-established, specific intermolecular interactions; consequently, each assembly contains a defined number of dendritic building blocks Such supermolecular dendrimeric structures have an equivalent degree of structural definition to a traditional covalent dendrimer; however, they are held together by reversible, nonbonded interactions.

Given the relative simplicity of using self-assembly as a noncovalent synthetic tool, this approach is relatively cost-effective, and its potential for genuine future applications is therefore significantly enhanced.

Surface-active amphiphilic molecules are well-known to assemble into discrete structures such as micelles and vesicles in water solution. Amphiphilic dendritic systems are not exception to this rule, and a range of dendrimers with surfactant-like assembly properties have been reported. Indeed, when mixed with water, the apolar and polar regions of these Janus-type molecules will attempt to phase separate via self-assembly into structures such as micelles. Importantly, only in some cases does the aggregation process give rise to true micellar structures: this occurs at molecular concentrations C greater than the so-called critical micellar concentration (CMC), which is one of the key parameters in self-assembly. When C > CMC, aggregates with a variety of different, non-micellar structures – often ill-defined – are formed. In other words, CMC defines the thermodynamic stability of the micelles. The latter is a very critical property in drug-delivery applications of micelles because intravenous injection of micellar solutions are associated with extreme dilutions by circulating blood (usually about 25-fold dilution at bolus injection or a much higher dilution at infusion). If the concentration of a micelle forming molecule in the circulation drops below the CMC, the micelles may be prematurely destroyed, resulting in the release of their cargo into the bloodstream before it reaches its target. This, in turn, will not only result in a poor therapeutic regime but, perhaps more importantly, could be dangerous because off-target and other unwanted side effects might (and likely will) originate. On the other hand, amphiphilic compound concentration cannot be increased above some critical values that correspond to the onset of micellar aggregation and precipitation, provoked by the interpenetration of the hydrophilic micellar coronas.

DNA Goes Curvy! (Or Effect of Self-Assembled Dendritic Nanovector Morphology on DNA/RNA Binding)

With the self-assembly concept as a guiding inspiration, Smith *et al.* reasoned that rather than using covalent synthesis to put the multivalent array in place, simple dendron self-assembly processes could achieve the same goal, with the self-assembled dendrimers behaving somewhat like a higher generation covalently constructed system [33]. In other words, they considered that, by combining simple dendron chemistry with self-assembly, they could achieve a cost-effective approach to tunable nano-assemblies with high-affinity for biological targets. Thus, in 2008 Smith and coworkers made a preliminary report of the synthesis of dendrons Z-G1-SP, Z-G2-Sp, Chol-G1-SP, Chol-G2-SP and $Chol_2$-G1-SP Fig. (**13**), and their application in the binding of DNA and its delivery into cells [37].

From their experiments it was evident that when there is a simple Z-protecting group at the focal point, in the case of Z-G2-SP a smaller amount of amine was required to condense the DNA, and that it was therefore a significantly more effective DNA binder than Z-G1-SP [37]. This evidence was in agreement with the undelying hypothesis that the surface spermine groups act as a multivalent array and collaborate in binding the DNA, with the presence of more surface ligands enhancing binding, as further supported by our atomistic molecular modeling simulations [39, 40]. However, when a cholesterol unit was placed at the focal point of the dendron, both Chol-G1-SP and $Chol_2$-G1-SP were found to be much more effective DNA binders than their second generation analogue Chol-G2-SP – i.e., less is more – even though the cholesterol unit could not be directly involved in forming interactions with the DNA [38]. It is also worth noting that whilst changing the Z group for a cholesterol unit significantly improved the DNA binding of the G1-SP dendrons, the same structural modification had a lesser effect on the binding ability of the G2-SP dendrons. At the same time, from the standpoint of gene delivery, compounds Z-G1-SP and Z-G2-SP both required the addition of chloroquine (a known endosomal escape enhancer) in order for transfection to be observed. However, the cholesterol-modified derivatives were better in terms of gene delivery: although compound Chol-G1-SP still required the addition of chloroquine, it demonstrated quite effective gene delivery, while Chol-G2-SP and $Chol_2$G1-SP showed very good levels of transfection even in the absence of chloroquine.

Importantly, the nature of this binding and transfection enhancement for Chol-G1-SP *cannot* be meaningfully modeled using simple atomistic molecular dynamics methods [39, 40] - e.g., 1:1 dendron:DNA complexes - because the spermine-functionalised surfaces of Z-G1-SP and Chol-G1-SP are, in their own right, identical, yet the degrees of binding are very different. This is a prototypical example in which the atomistic-scale MD simulations clearly reach and show all their own limits; thus, moving along the x-axis in Fig. (**2**) – that is, switching to higher scales, mesocopic simulations – becomes an obligatory choice to unveil the reasons of these intriguing findings.

To explain all the exciting properties summarize above, Smith then hypothesized that the hydrophobic units were able to self-assemble, and hence generate multivalent arrays of spermine ligands *in situ*, and that therefore Chol-G1-SP was more effective than Z-G1-SP [38]. However, there were a number of interesting experimental observations which he and collaborators were unable to fully explain. In particular, they could not rationalize the reasons why i) lower generation Chol-G1-SP compounds were more effective DNA binders than their higher generation Chol-G2-SP analogue – even though they have fewer spermine ligands on their surfaces, and ii) $Chol_2$G1-SP was significantly more effective in

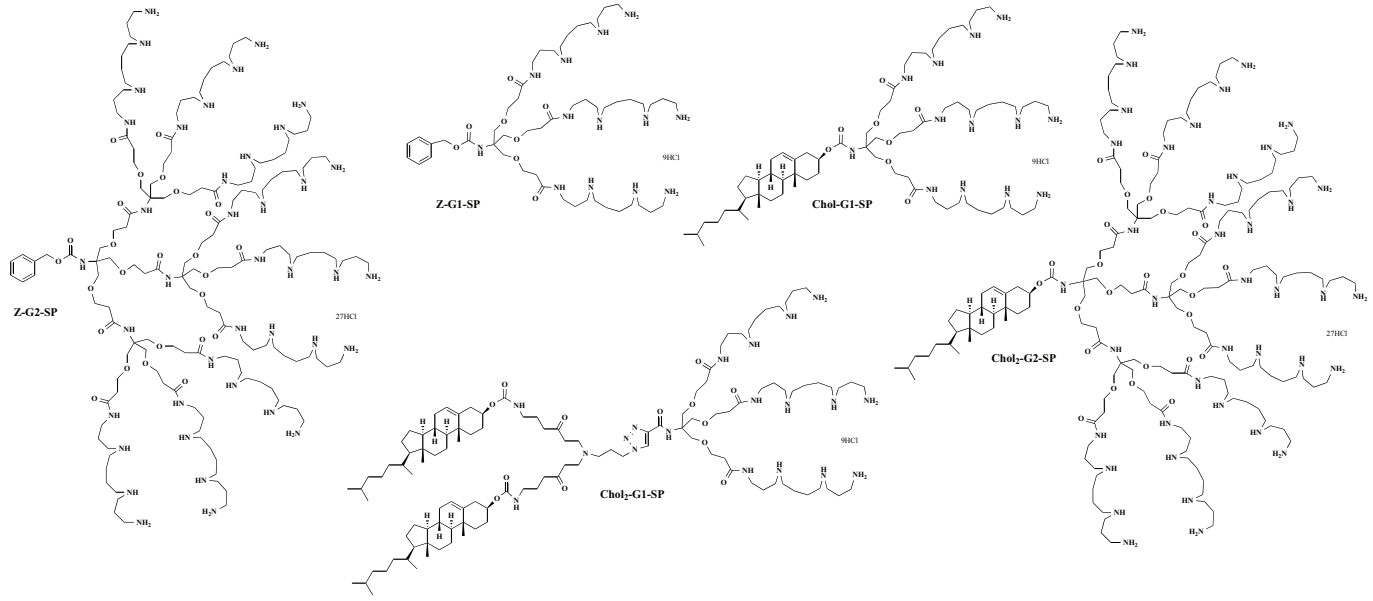

Fig. (13). Spermine-based dendrons modified at their focal core with different hydrophobic units. Adapted from [38], with permission of the RSC.

terms of gene delivery into cells than the Chol-G1-SP which, said it in other words, sounds like "how does the extra cholesterol unit assist gene delivery?"

In trying to find molecular-based answers to Smith's conundrums, we initally modelled Chol-G1-SP and Chol-G2-SP using multiscale modeling in the absence of DNA with the purpose to gain an insight into why Chol-G1-SP unexpectedly showed greater affinity for DNA, even though it has fewer spermine surface ligands [38]. Mescoscopic simulations according to our multiscale recipe immediately revealed that the self-assembly of these of Chol-G1-SP ligands into aggregates in water was a thermodynamically favored process. Interestingly, moreover, an increase of the dendron concentration in solution reflected only in a corresponding increase of the aggregates number but did not alter significantly their morphology or their composition. At first sight, the modeling of Chol-G2-SP yielded similar results: spherical aggregates were formed, driven by the hydrophobicity of the cholesterol units, which can lower their energy by phase separating from the aqueous phase.

Following the expectations stemming from geometrical considerations, both Chol-G1-SP and Chol-G2-SP predominantly form spherical monodisperse micelles with average diameters of 3.4 and 3.8 nm, respectively. However, the effective greater degree of hydrophobicity of $Chol_2$-G1-SP and a reduced like-charge repulsion in the dendritic cationic headgroup exerted by the ionic strength encourages phase change in the nature of its aggregate, ultimately resulting in cylindrical micelles see Fig. (**14**).

Classically, assembly geometries for amphiphilic molecules is dictated by the proportions of their polar and apolar domains, aptly described by the so-called packing parameter $P = v_h/a_0l_c$ [41], in which v_h is the volume of the densely packed hydrophobic segment, a_0 is the effective cross-sectional area of the hydrophilic group, and l_c is the chain length of the hydrophobic moiety normal to the interface. Based on simple geometric considerations of micellar core volume *vs*. surface area, it is easy to show that $P < 1/3$ is characteristic of spherical micelles, $1/3 < P < 1/2$ characterizes self-assembly of cylindrical shape, $1/2 < P < 1$ corresponds to vesicles, flat lamellae are formed at $P = 1$ and, lastly, inverted micelles are expected for $P > 1$.

Elementary molecular modeling considerations allowed us then to calculate the packing parameter for all Chol-based dendrons in hydrated conditions: P values of 0.24 and 0.12 were thus obtained for Chol-G1-SP and Chol-G2-SP, respectively, while the estimated value for for $Chol_2$-G1-SP P = 0.47 indicated the formation of cylindrical micelles for this molecular series. This theoretical prediction were found to be fully in line with the corresponding system morphologies discovered by our mesoscale simulations, as seen in Fig. (**14**).

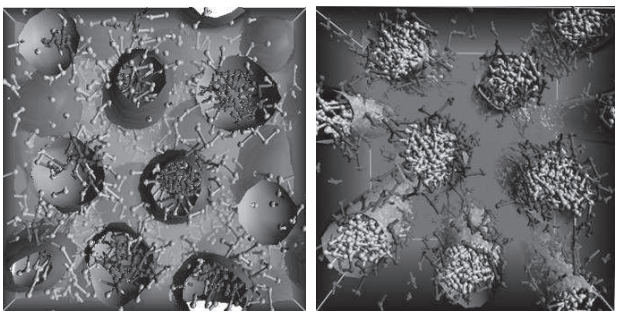

Fig. (14). Mesoscale modeling of amphiphilic dendrons Chol-G1-SP (left) and $Chol_2$-G1-SP (right) showing aggregation into spherical and cylindrical micellar objects, respectively. In all pictures, the sticks represent the dendron beads while light to dark gray surfaces are adopted to highlight the various hydrophobic regions. The gray field is finally used to represent water.

When modeled in the presence of DNA, all three dendrons retained their distinctive modes of self-assembly: a neat tendency for the DNA to wrap itself around the dendron aggregates could be detected but, interestingly, different mechanisms and, hence, different overall structures ultimately resulted. As highlighted in Fig. (**15**), in the case of the spherical micellar systems, the DNA molecules loosely packed without a well-defined inter-helical pattern or distances. The micelles appear to undergo a small degree of deformation in the complexes, with a tendency to elongate along the DNA longitudinal direction presumably to enhance the adhesion with the rather planar, extended surface of DNA. In these cases, the DNA molecules seem to comply with the well-known "bead-on-a-string" model, according to which some regions of the nucleic acid are engulfed by the micelles (see left panel of Fig. (**15**)) whilst some others are no longer surrounded by them. Thus, the DNA helices are partially embedded within the micellar organization and partially exposed to the solution environment, where Na^+ ions

originating from the electrolyte provide the charge neutralization required for eventual condensation.

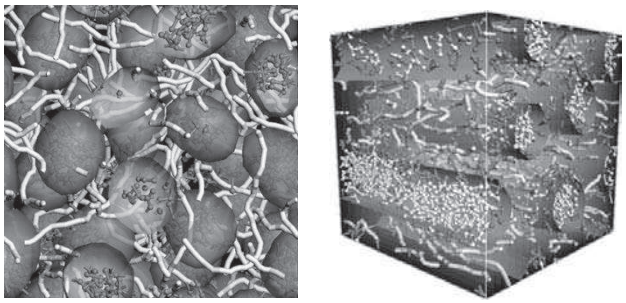

Fig. (15). Mesoscale modeling of the interaction between DNA and the aggregates of Chol-G1-SP (left) and $Chol_2$-G1-SP (right). Graphical scheme as in Fig. (**14**).

To a first approximation, the average number of DNA base pairs covered by the Chol-G1-SP and Chol-G2-SP micelles Fig. (**14**) can be estimated by resorting to the simple relationship: $n_{bp} = D_m/(3.4)\times 10$ where D_m is the spherical micelle diameter, 3.4 is the DNA duplex pitch (in nm) and 10 is the number of base pairs per duplex pitch. Inserting the estimated values of D_m of 3.4 and 3.8 in the above expression for n_{bp} yields $n_{bp} = 10$ for Chol-G1-SP and $n_{bp} = 11.2$ for Chol-G2-SP. It must be noted here that, considering the mismatch between the surface curvature of DNA and that of the micelles, the corresponding 20 (or 22.5) DNA phosphate groups per micelle are, however, not all bound directly to the micelles themselves even though the dendritic micelles may elongate slightly along the DNA chain axis to maximize the favourable electrostatic interactions.

As clearly shown by the DPD simulations, dendron $Chol_2$-G1-SP originate a cylindrical micellar morphology in which the DNA chains insert into the regular interspace of the cylinders. We note that such a system would be expected to (i) bind and compact DNA efficiently, (ii) protect DNA from degradation, (iii) achieve efficient DNA release, as verified by the corresponding experiments. It is generally known that the DNA double helix behaves as a semi-flexible coil; thus, the cylindrical shape of the micelles formed by $Chol_2$-G1-SP is better able to comply with the wrapping pattern of the semi-rigid DNA helix than the small sperical micelles generated by the other dendrons. As can be easily understood from the right panel of Fig. (**15**), this mesoscopic organization of $Chol_2$-G1-SP with DNA results in more efficient and well-organized DNA compaction and, hence, potential protection from degradation during DNA delivery.

Applying the same calculations for the estimation of the average number of DNA base pairs covered by the micelles to the case of $Chol_2$-G1-SP system yields a value of n_{bp} of 44.7. In line with the foregoing discussion, the cylindrical shape of the resulting $Chol_2$-G1-SP dendron aggregates, although having overall lower surface charge density ($\sigma_m = 1.7$ e/nm^2), can not only exploit the surface charge distribution more efficiently by following the seemingly cylindrical shape of the semi-rigid DNA duplex, but can also complex a considerably larger number of DNA bases per aggregate with respect to its less hydrophobic counterparts.

These morphological proposals also provide a rationale for the results of the enhanced affinity towards DNA experimentally detected for $Chol_2$-G1-SP ($CE_{50} = 0.49$) with respect to the other two nanovector counteparts ($CE_{50} = 0.52$ and 1.35 for Chol-G1-SP and Chol-G2-SP, respectively) [38]. It might be of use to recall here that CE_{50} represent the charge excess (or N:P ratio) required to displace 50% of EthBr in the corrsponding assay. In the case of the assembled systems characterized by smaller micelles (i.e., Chol-G1-SP and Chol-G2-Sp), our simulatuions clearly showed that the overall DNA surface is less covered (patch-like coverage) which allows for better residual binding of small molecules like EthBr. Therefore, in order to "fill the gaps", higher concentrations of dendrons are necessary to attain the same result displayed by the cylindrical micelles formed by $Chol_2$-G1-SP. At the same time, however, Chol-G1-SP has a significantly higher surface charge density than $Chol_2$-G1-SP (for which $N_{agg} = 34$ and $\sigma_m = 1.7$ e/nm^2) and this effect partly compensates for the 'patchy' DNA covarage of Chol-G1-SP, making it comparable as a DNA binder to its more hydrophobic counterpart, $Chol_2$-G1-SP.

A Trick of the Tail (Or Structure-Activity Relationship Development for Self-Assembled Dendron-Based Nanovectors)

Enticed by the encouraging – and somewhat surprising – results presented above, in order to expand the possibility and the variety of these assembled dendron nanovectors, our jointed groups then decided to study if and how a variation in the structure of the hydrophobic unit could reflect in a modification of the DNA binding capacity and gene delivery performance of this class of dendrons see Fig. (**16**). Accordingly, a series of dendrons with a variety of lipophilic units at their focal points were synthesized and tested for DNA binding and transfection capacities, revealing another set of stimulating evidences: not only all modified dendrons were able to tightly bind DNA and efficiently transfect cells, but for the first time and with the aid of multiscale molecular modeling a structure-activity relationship (SAR) could be formulated between the DNA binding affinity and the overall surface charge σ_m of the micellar assemblies but, perhaps more importantly, the SAR could be extended to cellular gene delivery, as σ_m plays a fundamental role in controlling the extent of the endosomal escape (*vide infra*) [42].

Thus, state-of-the-art multiscale simulation techniques were employed to monitor the dendrons self-assembly processes and to gain an insight into the types of aggregates eventually formed. First of all, the simulations revealed that all hydrophobically modified dendrons of generation 1 were able to form spherical supermolecular structures see Fig. (**17**) with diameters D_m in the range of 3 -5 nm see (Table **4**).

The spherical geometry of the self-assembled supramolecular entities is a direct consequence of the conical molecular shape of each dendron, featuring a relative large cationic head and a comparatively small lipophilic part. Let us then recall Israelachvili's rules for P value calculations presented above [41], and consider a generic micelle with a core radius R_c, and made up of N_{agg} molecules. By simple geometrical principles, then, the volume V_c of the micellar core can be obtained as $V_c = N_{agg}V_h = 4\pi R_c^3/3$, , the surface area of the core as $A_c = N_{agg}a_0 = 4\pi R_c^2$ and, finally, the value of the micellar core radius as $R_c = 3v_h/a_0$. If the micellar core is densely packed with the hydrophobic moieties filling the entire space, then the radius of the micelle core cannot exceed the fully extended length of the hydrophobic portion. Introducing this constraint into the expression for R_c, we then arrive at the above stated condition $0 \leq P \leq 1/3$ if an amphiphile is to form a spherical micelle.

By coupling basic molecular modeling concepts to the dimensional micellar parameters estimated by mesoscopic simulations and listed in the first three columns of (Table **4**), we were able to calculate the corresponding value of packing parameter P for all modified dendrons under hydrated conditions. A cursory glance at the P values in (Table **4**) reveals that in all cases these numbers fall between 0.24 and 0.32, in agreement with the corresponding spherical morphologies predicted by our mesoscopic simulations.

The mesoscale simulations of these dendron micelles carried out in the presence of DNA neatly show that, in all cases, the overall systems consist of parts of free, unfolded, single-chain DNA that

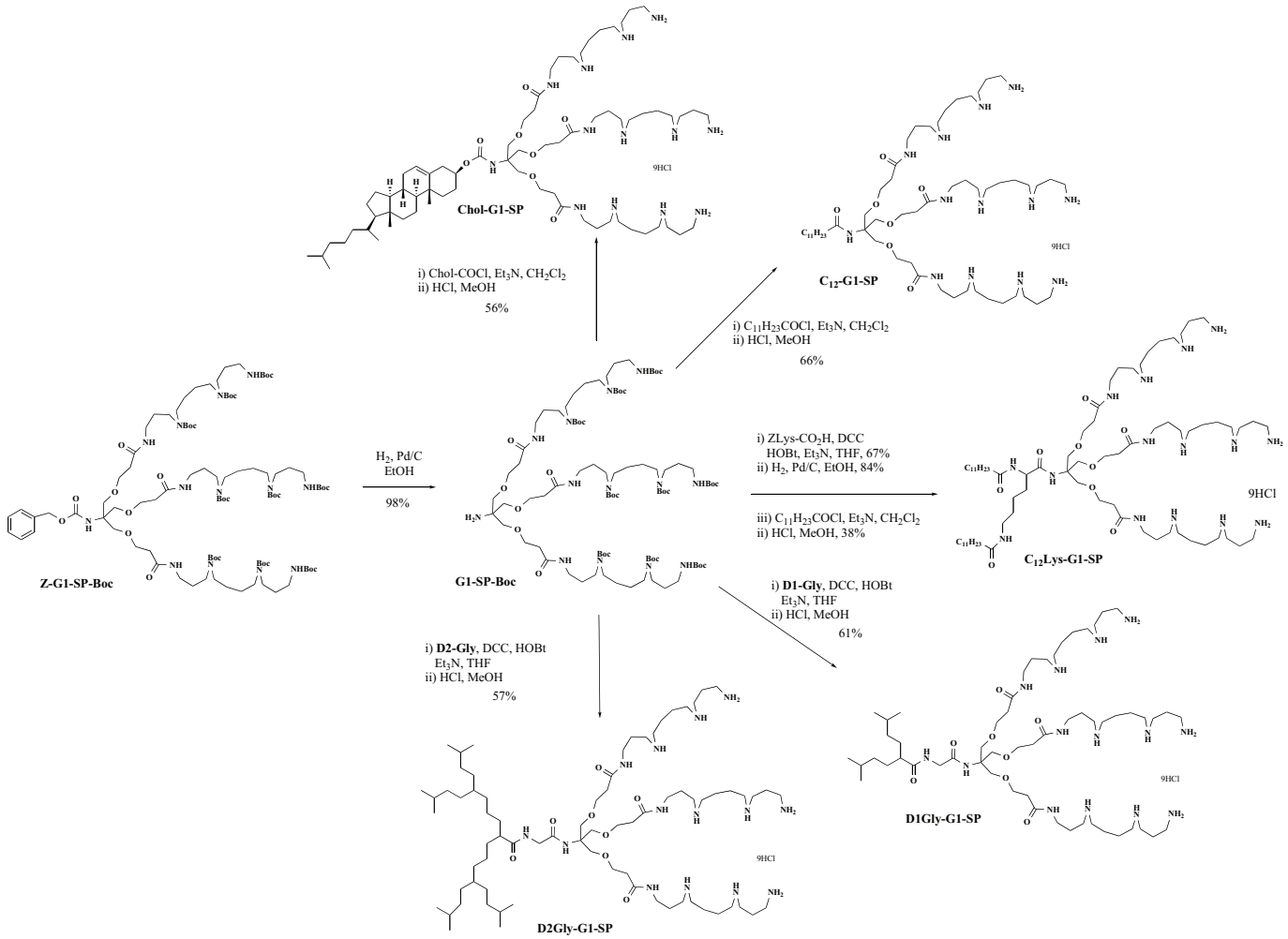

Fig. (16). Synthetic pathway of first generation dendron-based nanovectors with different hydrophobic groups at the focal point. Adapted from [42], with permission of the ACS.

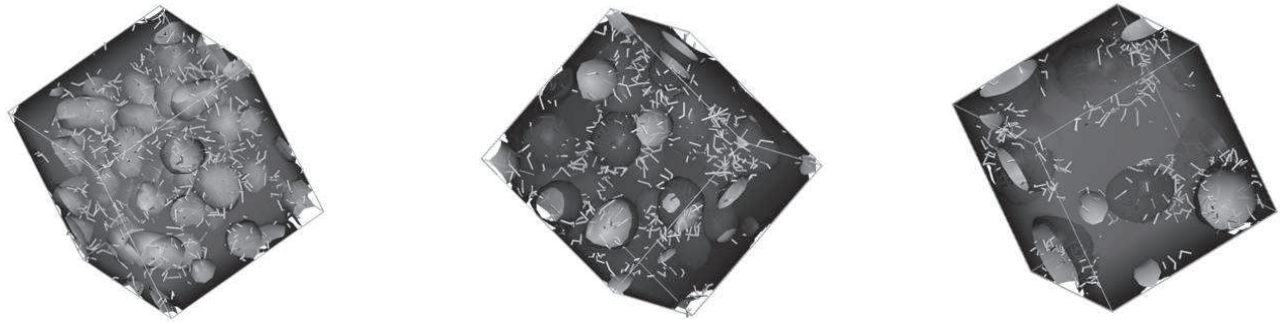

Fig. (17). Mesoscale modeling of amphiphilic dendrons showing aggregation into spherical micellar objects. (Left) Chol-G1-SP; (middle) C_{12}-G1-SP; (right) D_2Gly-G1-SP. In all pictures, the light gray sticks represent the dendron head groups while light to dark gray spheres are adopted to portray the various hydrophobic regions. The gray field is finally used to represent water. Adapted from [42], with permission of the ACS.

connect micelles on which a partial amount of DNA has been adsorbed see Fig. (**18**). In other words, all dendron/DNA complexes present a typical *beads-on-a-string* structure, made of dendron micelles connected by a DNA thread. Importantly, this predicted morphology is supported by detailed AFM studies between G4 PAMAM dendrimers and DNA [43] – indicative that these self-assemblies of dendrons can be considered to be somewhat like covalently bound higher generation spherical dendrimers. These structures are also somewhat reminiscent of the structure of open chromatin, which consists of an array of nucleosome core particles, separated from each other by up to 80 base pairs of linker DNA [44]. However, in clear contrast to the periodic structure of open chromatin, the dendron micelles appear to be distributed in a non-periodic, more irregular way.

Less is More: The Importance of Being Coulomb (Or Charge Density Effects in Self-Assembled Dendrons)

So far we have seen that, according to the characteristic P value, hydrophobically modified dendrons can self-assemble into differntly shaped micelles. In particular, both Chol-G1-SP and Chol-G2-SP modified dendrons predominantly form spherical

Table 4. Values of the Micellar Diameter D_m (nm), Core Radius R_c (nm), Aggregation Number N_{agg}, Packing Parameter P, and Micelle Surface Charge Density σ_m (e/nm^2) for the Different Modified Dendrons (Figure 16) As Obtained from Mesoscale Simulations. Adapted from [42], With Permission of the ACS

Compounds	D_m	R_c	N_{agg}	P	σ_m
Chol-G1-SP	3.4 ± 0.1	0.8	21	0.24	5.2
C_{12}Lys-G1-SP	4.0 ± 0.2	1.3	24	0.24	4.3
D2Gly-G1-SP	4.9 ± 0.2	1.5	32	0.32	3.8
C_{12}-G1-SP	4.0 ± 0.1	1.3	16	0.28	2.8
D1Gly-G1-SP	4.0 ± 0.2	0.9	12	0.25	2.1

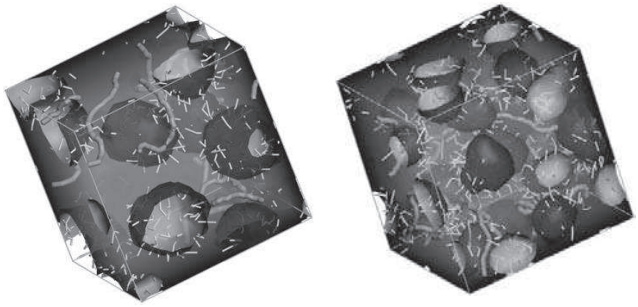

Fig. (18). Mesoscale modeling of the interaction of DNA with the amphiphilic dendrons D_2Gly-G1-SP (left) and C_{12}-G1-SP (right) as an example. In all pictures, white sticks represent dendron head groups. Dark gray spheres are adopted to represent the various hydrophobic regions along the series. A light gray field is used to represent water. DNA molecules are depicted as light gray sticks. Adapted from [42], with permission of the ACS.

monodisperse micelles with average comparable dimensions. However, when the aggregates of Chol-G1-SP and Chol-G2-SP are considered in more detail, a significant difference between them arises. Fig. (**19**) represents the effective positive charge density on the surfaces of these hydrophobically modified dendron aggregates. Clearly, Chol-G1-SP gives rise to a more highly charged aggregate (left panel) than Chol-G2-SP (right panel). This may seem counterintuitive, because Chol-G2-SP has twenty seven protonatable amine groups on the surface, whereas Chol-G1-SP only has nine. However, the self-assembly process is significantly more effective for Chol-G1-SP than the Chol-G2-Sp analogue, and this means that Chol-G1-SP gives rise to a much more effectively packed aggregate with a tightly packed positively charged surface. Conversely, for the aggregates of Chol-G2-SP, the surface charge is spread more diffusely.

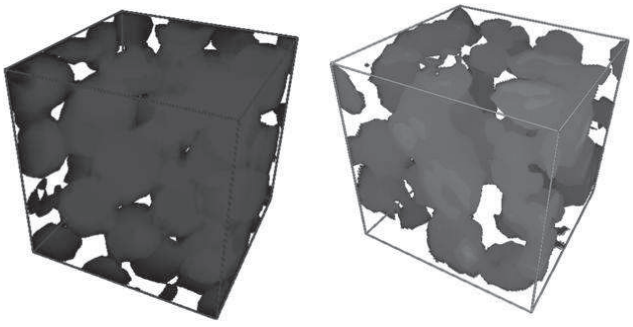

Fig. (19). Rendering of the surface positive charge of the Chol-G1-SP (left) and Chol-G2-SP (right) micelles. The darker gray tone of the spheres used to portray the charge distribution, and their higher number clearly testify the significantly greater charge density of this system with respect to its counterpart. Adapted from [38], with permission of the RSC.

Quantitatively, this argument is supported by the estimation of the numerical values of the surface charge densities σ_m for both micellar systems. In the case of Chol-G1-SP, the aggregation number estimated from the mesoscopic simulations, $N_{agg} = 21$, leads to a σ_m value of 5.3 e/nm^2, whilst for Chol-G2-SP $N_{agg} = 7$ and, hence, $\sigma_m = 4.2$. In this way, we propose that self-assembly controls the surface charge of the aggregate, and hence the relative affinities of these systems for DNA. Under this sperpective, less is more, and the smaller dendron is actually better able to bind DNA once the multivalency becomes expressed on the nanoscale through dendron self-assembly.

Let us now consider the influence of the different tail architecture on this fundamental property. In practical terms, σ_m can be thought of as a measure of how positively charged a micelle is. Two micelles containing the same number of dendrons, and therefore carrying the same overall charge, may exhibit different values of σ_m, if the micelle sizes, and hence their surface areas, are different. To calculate σ_m we therefore need to know the aggregation number of the micelle N_{agg}, the charge of each dendron head, and the micellar surface area $Sm = 4\pi R$, as $\sigma_m = e \times N_{agg}/S_m$. Using again the data reported in (Table **4**) and the constant value of +9 for the overall charge of each dendron headgroup, the σ_m values shown in the last column of (Table **4**) could be easily estimated.

Summarizing the overall evidence stemming from the analysis of data in (Table **4**), as obtaiend from the application of the multiscale molecular modeling recipe, led to the following, important considerations:

- The overall series of spermine-based amphiphilic dendrons assemble into small, spherical micelles in water and in the presence of physiological ionic strength conditions (150 mM), as experimentally verified for similar systems.
- The different architectures of the hydrophobic portion resulted in differently sized micelles and/or a different number of dendrons per micelle N_{agg}, and, hence, a different micellar surface charge density σ_m.

Most importantly, the experimentally verified CE_{50} values directly correlate with the surface charge density values σ_m estimated from the multiscale simulations, indicating that the micelles characterized by higher values of σ_m (i.e., Chol-G1-SP, C_{12}Lys-G1-SP, and D_2Gly-G1-SP) are tighter DNA binders than their counterparts with lower σ_m values (i.e., C_{12}-G1-SP and D_1Gly-G1-SP). Interestingly, comparing the best DNA binders, Chol-G1-SP, C_{12}Lys-G1-SP and D_2Gly-G1-SP, the former compound assembles into micelles of much smaller diameter than the latter two. This is presumably due to the less sterically demanding nature of cholesterol leading to more effective packing within the micellar interior, compared with the branched hydrophobic units in the latter two dendrons, which will not be able to pack so efficiently. As such, even though the micelles formed by Chol-G1-SP contain fewer dendron units and have less total positive charge than the micelles formed by

C_{12}Lys-G1-SP and D_2Gly-G1-Sp, their smaller size means that they have significantly higher surface charge density, and as such, they are therefore much more effective DNA binders.

The Long and Winding Road (Or Aspects of DNA/RNA Bending Around Self-Assembled Nanovectors)

When considered in complex with DNA, all these hydrophobically modified dendron systems, but particularly in the case of C_{12}-G1-SP and D_1Gly-G1-SP, DNA localizes in the interstitial space and eventually associate into small bundles. This might, at first sight, be an unexpected phenomenon. However, DNA bundles may originate from a subtle interplay of the salt-induced screening of the electrostatic interactions and the *depletion-attraction* caused by the dendron micelles. Depletion-attraction is a somewhat underappreciated force associated with the aggregation of two large colloidal objects as a consequence of the osmotic pressure generated by the exclusion of smaller objects from their interacting interface [45]. While depletion-attraction has previously been reported for like-charges or neutral objects, the screening of the electrostatic interactions enables this effect to be observed also between DNA and the oppositely charged dendron micelles, for which the electrostatic interactions are attractive. The presence of salt therefore facilitates bundling of DNA by reducing the electrostatic repulsion between DNA molecules, and also reduces the electrostatic attraction between positively charged micelles and negatively charged DNA. The existence of DNA bundles and condensed regions can also be understood by taking into account the small dimensions of the micelles formed by all these dendrons and the relevant values of σ_m. Indeed, extensive wrapping of DNA around small micelles will result in a quite high cost of DNA bending (or elastic) free energy; accordingly, this is not observed in any of the considered systems discussed above. Furthermore, a decrease of the DNA adsorbed amount per particle is observed as the surface charge density, σ_m, decreases. This is only partly compensated by the fact that some of the free part of DNA adsorbs on new particles, and therefore the bundling of unbound DNA becomes more favored.

We can go deeper into these concepts by considering that, in aqueous solutions, both DNA and dendron micelles are associated with their respective counterions. The high charge density of DNA actually results in counterion condensation: in its solution structure, the base length between negative phosphate groups on the DNA backbone is equal to $l_0 = 1.7$ Å. This is significantly less than the Bjerrum length in water $\lambda_B = e^2/\varepsilon_w k_B T = 7.1$ Å, where ε_w is the dielectric constant of water (= 80), k_B is the Boltzmann constant, and T is the temperature. The Bjerrum length corresponds to the distance where the Coulomb energy between two unit charges is equal to the thermal energy k_BT. Under these conditions, it has been shown that positive counterions will condense on the DNA backbone until the Manning parameter $\xi = l_0/l^*$ approaches unity, l^* being the renormalized distance between the negative charges after counterion condensation [46]. A similar analysis shows that near the surface of a positively charged micelle, almost half of the negative counterions are contained within the so-called Gouy-Chapman length $l_{G\text{-}C} = e/2\pi\lambda_B\sigma_m$. Combining DNA and our amphiphilic dendron micelles allows the charges of the spermine head groups to neutralize the phosphate moieties on DNA. This replaces and releases the tightly bound-counterions of both micelle and nucleic acid in solution. The resulting gain of translational entropy by the counterions is a driving force for higher order self-assembly into micelle/DNA complexes [47]. It should be pointed out that the term bound counterions is used in a loose form: indeed, the counterions near the DNA or a micelle surface are bound and yet remain in their fully hydrated state. This implies no change in the entropy of water molecules upon release of bound counterions into solution. The driving force of the counterion release mechanism is reduced by added salt, as in the experiments and simulations described in this work. This is particularly true for counterion release from the dendritic micellar assembly, which relies on a concentration gradient between the layer of ions confined close to the micelle and the bulk solution. Since $l_{G\text{-}C}$ scales with l/σ_m, the concentration of counterions next to each micellar entity scales with σ_m. Therefore, the addition of salt to a solution in which the complex between DNA and micelles are formed has a stronger effect on those complexes for which the micelles are characterized by lower values of σ_m. This is agreement with the present experimental evidence, for which the DNA binding ability of the amphiphilic dendrons, as quantified by the ethidium bromide assay, decreases with the decreasing charge surface density of the micelles.

Understanding the pathways and mechanisms governing the interactions of modified-dendrons/DNA complexes and cells is crucial to making dendron-mediated gene delivery therapeutically viable. The complexity of the transfection process – from initial attachment of a nanovector/DNA complex to the plasma membrane to internalization of the complex via endocytosis, its release from the endosome followed by the dissociation of the vector from the DNA, and finally the transport of DNA into the nucleus followed by successful gene expression – suggests that an interplay of many critically important parameters needs to be considered in order to achieve transfection. The nanoparticle surface charge density σ_m discussed previously is one such parameter, controlling at least some of the aspects outlined above. If cellular attachment and uptake were the only limiting transfection efficiency factors via a σ_m-dependent mechanism, a linear increase of the transfection efficiency with σ_m would be predicted. Furthermore, for complexes with low σ_m, the transfection ability is also limited by endosomal escape. This was substantiated by transfection experiments performed in the presence of chloroquine. These experiments indicated that complexes with higher σ_m should be more able to escape from endosomes. The escape from endosomes likely occurs via an activated fusion process of the oppositely charged endosome membrane and the micelle/DNA complex. The activation energy of this process can be written as $\delta E = ak - b\sigma_m$, where a and b are positive constants. The parameter k is the bending rigidity of the micelle, which is mainly determined by the hydrophobic portion of the molecule and the area per hydrophobic moiety. Bending or deformation of the micelle, as required by fusion, results in an energy cost proportional to k. Since the interacting entities during fusion are oppositely charged, the activation energy decreases with increasing σ_m, making fusion more likely, in keeping with the current experimental results. In these ways the modeling studies are in agreement with the experimental results of the transfection assays.

Waterworld 2 (Again on the Effect of Water on Self-Assembled Dendrons/DNA(RNA) Complexes)

We have seen how water and the environment it creates around the nanovectors alone or in complex with the nucleic acids exert a fundamental role in the performance of these systems. In the case of self-assembled entities this role is subjected to an additional, controlling variable, that is, the shape and size of the resulting self-assembled objects. Once again, multiscale molecular modeling can assist in this topic: indeed, it is not difficult to infer from images taken from mesoscale simulations that spherical micellar systems are characterized by a higher water content within the micellar interspace than cylindrical ones [38]. Again at first approximation, from an estimation of the average center-to-center distance of the cylinders $d_{cyl}/_{cyl} = 5.9$ nm, and some simple geometrical considerations, the volume fraction of water in the hexagonal lattice formed by $Chol_2$-G1-SP was calculated to be equal to 0.42. Although the same approach cannot be applied to the alternative micellar systems due to the absence of a long-range regular structure, the comparison of the density maps of water for the $Chol_2$-G1-SP/DNA and Chol-G2-SP/DNA systems supported this concept see Fig. (**20**). The higher water content in the Chol-G2-SP spherical micellar system may imply that a significant fraction of dendron and DNA charges

are wasted in terms of mutual interactions. This is in line witht the illustration in the right panel of Fig. (**15**), as a notable fraction of the periphery of the spherical dendron micelles fail to contact DNA and vice versa.

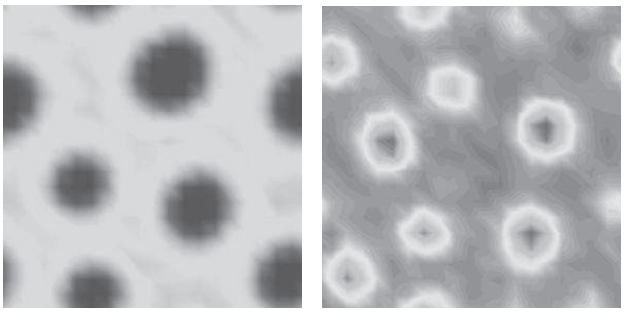

Fig. (20). Rendering of density distribution of water molecules in the $Chol_2$-G1-SP/DNA (left) and Chol-G2-SP/DNA (right) complexes. The higher level of intermicellar hydration is apparent in the Chol-G2-SP-based system, highlighted by the gray darker areas around the micellar objects.

Dangerous Liaisons (Or Critical Micellar Concentration Estimation Via Computer Experiments)

According to the classical laws of thermodynamics, the free energy of micellization ΔG_{mic} – i.e., the driving force that might eventually lead the amphiphilic molecules to spontaneously aggregate in water – can be expressed in the simple form $\Delta G_{mic} = -RTlnK_m$, where K_m is the equilibrium constant between the aggregated and free forms of the given amphiphile in the aqueous environment. For conditions near or above the CMC, it can be shown that the above expression for ΔG_{mic} can be approximated to the form $\Delta G_{mic} = RTln(CMC)$. Accordingly, once either ΔG_{mic} or CMC is known, the other parameter can be easily estimated through this simple, fundamental relationship.

From an energetic standpoint, the change in Gibbs free energy of transfer of a single amphiphilic molecule from the monomeric state to a micelle of aggregation number N_{agg}, that is ΔG_{mic}, can be modeled as consisting of a hydrophobic part, $\Delta G_{mic,h}$, and an electrostatic part, $\Delta G_{mic,e}$, so that $\Delta G_{mic} = \Delta G_{mic,h} + \Delta G_{mic,e}$. The hydrophobic part stems primarily from the favorable energy of transfer of the hydrocarbon moieties from the aqueous phase to the micellar phase, and, secondarily, from the unfavorable residual interfacial contact of water with the apolar components within the micelles. The electrostatic part of ΔG_{mic} arises from the repulsion between the ionic head groups within the micellar shell.

Following the theory originally proposed by Tanford [48] and subsequently modified by other authors [49], and using the information available from our multiscale simulations, we were able to calculate the values of ΔG_{mic} and the corresponding CMCs for the five modified dendrons of Fig. (**16**), as shown in (Table **5**). As can be seen from this Table, ΔG_{mic} at room temperature has large, negative values, indicating that micellization is a spontaneous and highly favorable process for all amphiphilic dendrons, although ΔG_{mic} decreases on going from Chol-G1-SP to D_1Gly-G1-SP. Since the head group architecture is the same in all amphiphiles, the main differential contribution to ΔG_{mic} must originate from the $\Delta G_{mic,h}$ term, which reflects differences in the size and structure of the hydrophobic component.

Typically, micellar aggregates have CMCs of the order of 10^{-3}-10^{-5} M, while lower CMCs, even down to the nanomolar range can be found for amphiphiles that form either membranes or cylindrical aggregates. Recently, however, electron microscopy experiments performed on cholesterol-porphyrin micelles revealed that these amphiphiles could form virtually monodisperse spherical aggregates with a diameter of approximately 7 nm and a CMC value of 11 nM [50]. Amphiphiles showing low CMCs tend to have relatively large hydrophobic segments, and this normally results in an assembly shape with a lower curvature. However, our series of modified dendrons combine a large hydrophobic portion with a very large head group, resulting in a roughly conical amphiphile. The size of the hydrophobic segment is responsible for the low CMCs, while the large size of the head group results in the spherical geometry of the assembly.

It is of particular interest to note that the predicted CMC values for C_{12}-G1-SP and D_1Gly-G1-SP lie above the concentrations of the DNA binding assays (i.e. low μm concentrations) – as such, it is possible that the relatively poor DNA binding ability of these compounds reflects the fact that they are not aggregated under the experimental conditions as a consequence of their relatively small hydrophobic segments. Although a word of caution is due about the fact that the calculated values of ΔG_{mic} and CMC are obtained using validated but simplified theoretical approaches, the trends exhibited by these parameters are in line with the experimental data. Indeed, we were able to carry out full experimental aggregation studies on a closely related set of hydrophobically modified dendrons, and for these systems, the *in silico* predictions of micelle diameters, charge densities and CMC values were closely mirrored by the experimental results, both in terms of trends and absolute values, thus strengthening not only the reliability of the entire computational procedure applied but, perhaps more importantly, validating its predictive capacity.

Do you Recognize Me? (Or Some More Computational Aspects of Self-Assembly and Nucleic Acid Binding of Dendrons with Different Focal Points)

Each part of a dendron can play a distinctive role in controlling the biological behavior. As we have been discussing so far, the judicious choice of a hydrophobic group at the dendron focal point can originate the controlled self-assembly into larger nanoscale aggregates, with the relative size of the hydrophobic and hydrophilic groups controlling the architecture of the resulting self-assembled structure [38, 42]. The multiple surface groups of a dendron constitute an optimum multivalent array for displaying bioactive ligands — such arrays significantly enhance the binding affinity for key biological targets as a consequence of the entropic bene-

Table 5. Predicted Free Energy of Micellization ΔG_{mic} (kJ/mol) and Critical Micelle Concentration CMC (μM) for the Different Modified Dendrons of Figure 18. Adapted from [42], With Permission of the ACS

Compounds	ΔG_{mic}	CMC
Chol-G1-SP	-87.56	0.021
C_{12}Lys-G1-SP	-80.42	0.089
D_2Gly-G1-SP	-77.97	0.15
C_{12}-G1-SP	-55.92	12.5
D_1Gly-G1-SP	-49.29	47.6

fits of ligand organization [31]. However, thinking in a reverse mode, it should be also possible to make a dendritic branched scaffold degradable; particularly, it could be designed in such a way that, over time or in the presence of specific biological stimuli, it degrades (possibly in a controllable and predictable way) into smaller subunits [51]. This can enhance the biocompatibility of the dendron, lower its toxicity, and limit its persistence in cells. Dendron degradation also disassembles the multivalent array and therefore acts as an effective way of "switching off " the multivalent binding effect, significantly decreasing the affinity of the system for the biological target [52, 53].

In recent years, to improve biocompatibility, the attention has turned to biodegradable dendron frameworks [52, 53] and in 2009, Smith *et al.* reported a simple system based on Frechet-type aliphatic ester dendrons [53] modified with spermine surface groups which exhibited multivalent binding and degraded such that DNA binding became disfavored *in vitro* [39, 40]. Following this preliminary work, and relying on the previous experience on the capacity to self-assembly these molecules are endowed with when bearing hydrophobic units at their focal point, we went further and changed the dendron surface groups as well, replacing them with a triamine see Fig. (**21**) [54], as this moiety has been previously reported to lower the toxicity of the dendron constructs [39]. The effect of these modifications on DNA binding and cellular gene delivery were assessed, and the degradation of the dendrons was monitored as well using an *in vitro* mass spectrometric assay.

Initially, we assessed dendrons aggregation in aqueous solution, using solubilization experiments with the hydrophobic dye Nile Red paralleled by multiscale simulations. The first two colums in (Table **6**) reports and compare the CMC values for the six dendrons investigated in this paper estimated from a plot of the fluorescence emission intensity of Nile Red at 635 nm versus log 10 [dendron] and by molecular simulations.

As can be seen from the data, the functional group at the dendron focal point has a profound effect on the dendron aggregation process. Control compound Z-G2 did not show any evidence of aggregation under the conditions assayed (up to 1 mM). For the alkyl chain modified dendrons, there is an inverse relationship between the length of the hydrophobic chain and the CMC value. As the hydrophobic chain increases in length from C_{12}-G2 to C_{16}-G2 to C_{22}-G2, the experimental CMC value drops from 208 to 2 μM, a consequence of more effective packing of the longer hydrophobic chains resulting in better self-assembly. Both cholesterol-functionalized dendrons exhibited similar CMC values of ca. 5 μM. Clearly, cholesterol is quite effective in encouraging the self-organization of these dendrons. From the simulation standpoint, with the exception of Z-G2, all the remaining dendrons self-assembled into nanoscale objects of spherical shape. Recalling the concept of the packing parameter P, in the present case for all modified dendrons the calculated P value is < 0.33, predicting that all dendrons but Z-G2 would self-assemble into spherical micelles, as can be observed in Fig. (**22**).

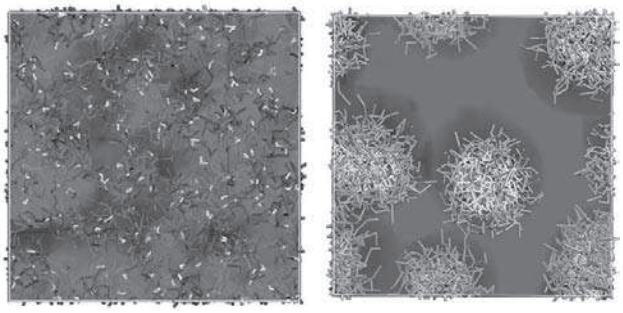

Fig. (22). Mesoscale modeling of Z-G2 (left) and Chol-G2 (right) dendrons in water. As can be clearly seen, Z-G2 molecules remain dispersed in solution whereas Chol-G2 self-assembly in well-defined spherical micelles. In both pictures, the hydrophobic portion of the dendron molecules is portrayed as white sticks while the hydrophilic heads are pointed in dark (Z-G2) and light (Chol-G2) gray sticks. A gray field is used to represent water. Redrawn from [54], with permission of the ACS.

It is fundamental to observe at this point that the CMC values predicted by simulation follow the correct, increasing experimental trend as the hydrophobic character of the dendron substituents decreases. Furthermore, one of the most critical parameter influencing the overall performace of these systems - the micellar surface charge density (σ_m) – is found to increase as the hydrophobic chain lengthens and becomes better able to pack, in agreement with corresponding measurements of zeta potentials (here not shown). Notably, even if these CMC values estimated *in silico* are to be taken with due caution, they are below the experimental concentrations employed in the transfection experiments, and the presence of micelles as nanovectors is therefore supported by the modeling.

Interestingly, the different architectures of the hydrophobic portion ultimately result in differently sized micelles and/or a different number of dendrons per micelle (N_{agg}) and, hence, a different micellar surface charge density σ_m. Comparing Chol-G2 and $Chol_2$-G2 with the other modified dendrons, we see that these compounds assemble into micelles of bigger diameters than the other counterparts. This is likely due to the highly hydrophobic nature of the flat, rigid cholesterol moieties leading to highly effective packing within the micellar interior. Also, comparing the two cholesterol-bearing molecules, modeling predicts the formation of larger micelles for $Chol_2$-G2 than Chol-G2. These larger aggregates are a consequence of the fact that a larger number of $Chol_2$-G2 are incorporated into

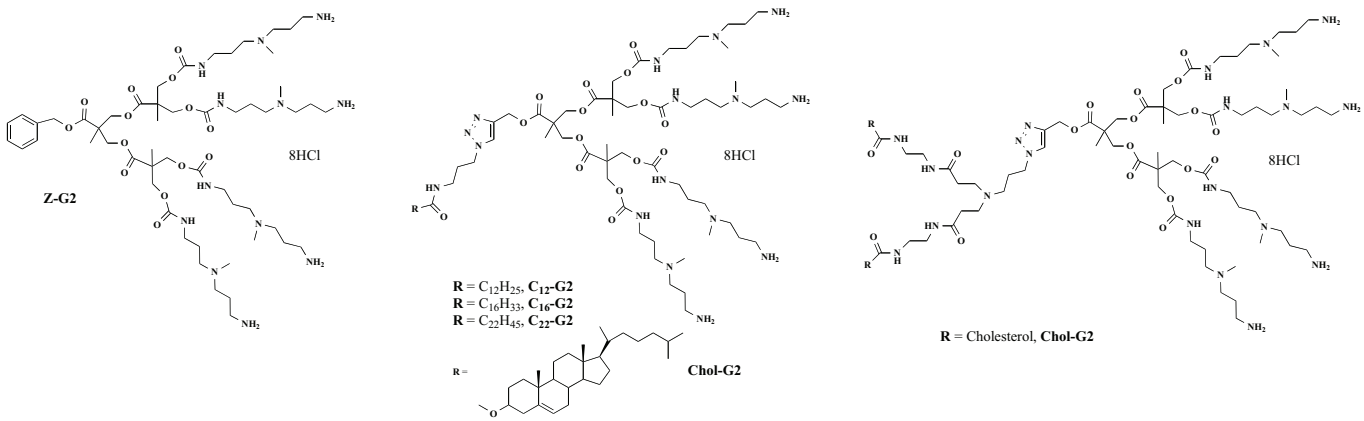

Fig. (21). New hydrophobically modified dendrons for self-assembly and controlled degradation. From [54], with permission of the ACS.

each micelle compared with Chol-G2 (22 molecules per micelle rather than 16) and due to the two cholesterol units at the focal point providing a more favorable free energy of micellization (by ca. 3 kJ/mol).

We then carried out a mesoscale modeling study of the interactions between DNA and the dendron micelles. The resulting morphology of the self-assembled micelles and DNA helices is visualized in the second panel of Fig. (**23**), while the first panel shows the corresponding, un-assembled Z-G2/DNA systems for comparison. As can be seen, in the presence of the dendron micelles the DNA molecules are loosely packed without a well-defined interhelical pattern or distances. As in the other examples discussed above, also in this cases the DNA molecules seem to comply with the "bead-on-a-string" model. The last panel of Fig. (**23**) shows the results obtained from the mesoscopic simulations performed on the PEI/DNA system, used as the gold standard comparison. These mesoscale results offer a sensible explanation for the high transfection capacity of PEI — the DNA is homogeneously intertwined between the PEI chains, so that it is quite efficiently protected from the outer environment. At the same time, since no particular structuring (e.g., beads-on-a-necklace) is attained in solution, there are some areas where DNA bundles appear and some free space which, ultimately, might yield better performance during release of this system.

Friend or Foe? (Or Computational Aspects of the Competitive Binding for Self-Assembled Dendrons by Nucleic Acid and Heparin)

Exploiting the morphological information on the self-assembled dendron micelles obtained at the mesoscale level, we then went back to atomistic simulations (step 3 in our computational recipe, *vide supra*); accordingly, a quantitative modeling of micelle/DNA interactions at a fully atomistic level was used to rank the affinity of each type of modified dendron micelle toward DNA, ΔG_{bind}. Interactions between the component of the micellar corona (outer dendron arms) and the grooves on the DNA double helix can be well seen in Fig. (**24**).

As shown in (Table **7**), the molecular dynamics-based MM/PBSA calculations indicated that $Chol_2$-G2 is by far the most effective DNA binder, followed by Chol-G2, C_{22}-G2, C_{16}-G2, and C_{12}-G2, in agreement with the corresponding experimental evidence. By considering the per charge normalized values of ΔG bind on the micelle ($\Delta G_{bind}/N$), it is clear that $Chol_2$-G2 is better able to utilize each charge in binding to the DNA double helix than Chol-G2 and all other self-assembled systems.

Focusing on the two tighter DNA binders, this observation, that $Chol_2$-G2 binds DNA more strongly than Chol-G2, is consistent with the corresponding experimental observations. This is perhaps surprising given that modeling indicated that the $Chol_2$-G2 self-assembled structures had lower surface charge densities than those resulting from Chol-G2 (Table **6**) and suggests that the larger micelle size of $Chol_2$ G2 (Table **6**) may play an important role in modulating the ability of the charges to bind to the DNA double helix without overcrowding at the micellar surface. Since PEI is a current standard vector system for DNA cell trasfection experiments, MD atomistic simulations were also run on a PEI/DNA for comparison. Interestingly, the estimated binding affinity of PEI toward DNA is, in terms of $\Delta G_{bind}/N$, somewhat intermediate between Chol-G2 and $Chol_2$-G2. This finding is indicative of the fact that both cholesterol bearing, self-assembling dendrons possess

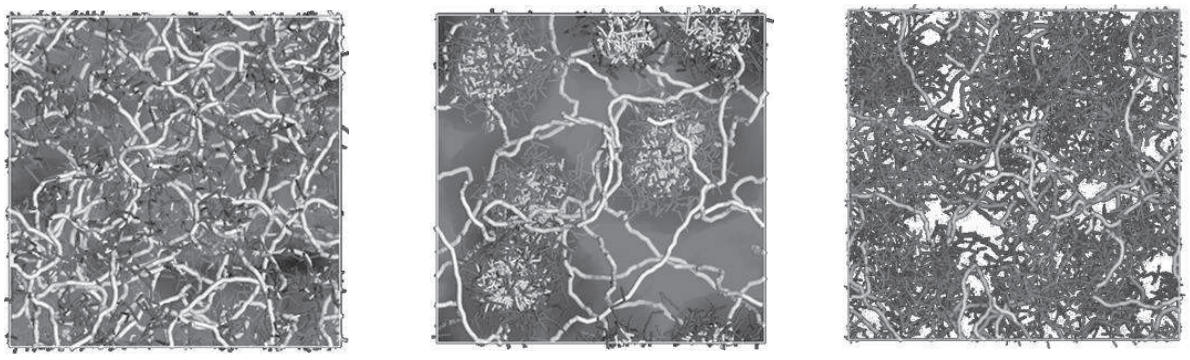

Fig. (23). Mesoscale modeling of Z-G2/DNA (left), Chol-G2/DNA (middle), and PEI/DNA (right) systems in water. As can be clearly seen, Z-G2 molecules remain dispersed in solution whereas Chol-G2 self-assembly in well-defined spherical micelles. The hydrophobic portion of the dendron molecules is portrayed as white sticks while the hydrophilic heads are painted in dark (Z-G2) and light (Chol-G2) gray sticks. Dark gray sticks are also used to depict PEI molecules. A gray or white field is used to represent water.

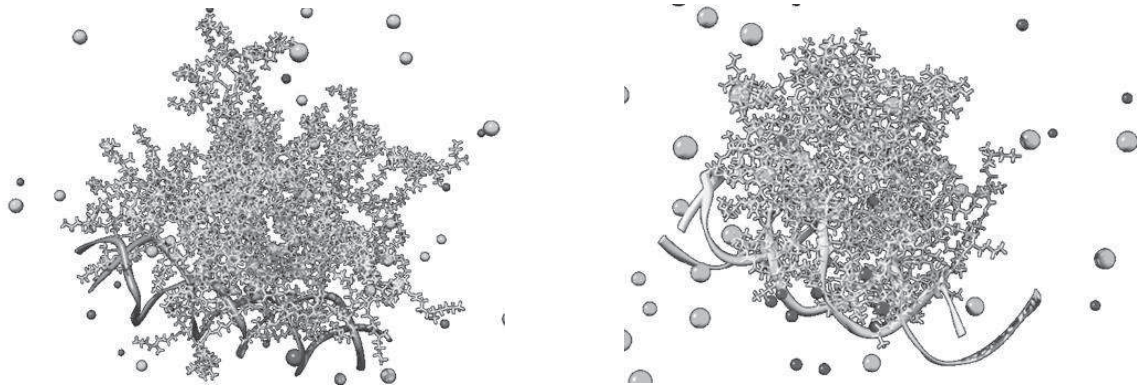

Fig. (24). Atomistic molecular dynamics simulation snapshots of the $Chol_2$-G2 (left) and Chol-G2 (right) micelle in complex with a fragment of DNA. The dendrons in the micelle are shown as light gray sticks, while the DNA fragment is in a ribbon representation. Cl^- and Na^+ ions are shown as light and dark gray spheres, respectively. Water is not shown for clarity. Redrawn from [54], with permission of the ACS.

Table 6. Values of the Experimentally Determined (CMC_{exp}) and Computationally Estimated (CMC_{sim}) Critical Micellar Concentration (μM), Micellar Diameter D_m (nm), Core Radius R_c (nm), Aggregation Number N_{agg}, Micelle Surface Charge Density σ_m (e/nm^2), and Free Energy of Micellization ΔG_{mic} (kJ/mol) for the Different Modified Dendrons in Figure 21 As Obtained from Mesoscale Simulations. Adapted from [54], With Permission of the ACS

Compound	CMC_{exp}	CMC_{sim}	D_m	R_c	N_{agg}	σ_m	ΔG_{mic}
C_{12}-G2	208 ± 56	2.7	2.9 ± 0.1	0.8	6	1.77	-63.6
C_{16}-G2	37 ± 6	0.23	3.1 ± 0.1	0.9	7	1.89	-75.7
C_{22}-G2	2.0 ± 0.1	0.080	3.3 ± 0.2	1.0	9	2.09	-92.3
Chol-G2	4.9 ± 0.6	0.035	3.9 ± 0.2	1.1	16	2.68	-96.4
$Chol_2$-G2	4.9 ± 0.6	0.018	5.1 ± 0.1	1.5	22	2.15	-99.6

Table 7. Free Energy of Binding ΔG_{bind} (kcal/mol) and Normalized Free Energy of Binding Per Charge on the Micelle $\Delta G_{bind}/N$ (kcal/mol) the Between Hydrophobically Modified Dendron Micelles and DNA. Adapted from [54], With Permission of the ACS

Compound	ΔG_{bind}	$\Delta G_{bind}/N$
C_{12}-G2	-16.8 ± 1.3	-0.35 ± 0.03
C_{16}-G2	-22.4 ± 1.7	-0.40 ± 0.03
C_{22}-G2	-33.8 ± 2.8	-0.47 ± 0.04
Chol-G2	-71.2 ± 3.1	-0.56 ± 0.02
$Chol_2$-G2	-119.2 ± 3.1	-0.68 ± 0.02
PEI	-269.0 ± 2.6	-0.63 ± 0.01

excellent DNA binding properties which could be potentially exploited with success in gene delivery processes.

We then went on to investigate the ability of these dendrons to transfect cells using a luciferase expression assay. From the transfection data, we saw that Chol-G2 was the most effective vector, with an activity of around 10% of that of PEI. $Chol_2$-G2 showed some transfection at ca. 4% PEI positive control, C_{22}-G2 only showed negligible levels, while Z-G2, C_{12}-G2, and C_{16}-G2 exhibited no measurable transfection.

Interestingly enough, the value of one of the micellar key parameters, the surface charge density σ_m, as estimated by our modeling procedures, correlates directly with the cellular transfection efficiency (TE) data discussed above. Indeed, the higher the value of σ_m, the higher the transfection efficiency of the corresponding system. This finding is not only qualitatively but also quantitatively in agreement with what is observed for cationic lipid/DNA-mediated delivery systems for which — depending on the morphological structure of the overall assembly — high values of σ_m are beneficial for achieving high TEs.

Overall, however, none of the new dendrons performs as well as PEI. Since efficient DNA binding, cellular uptake, endosomal escape and toxicity causes were excluded by experiments, we reasoned that although our dendrons self-assemble into highly effective multivalent DNA binders perhaps this binding was in fact too strong to facilitate intracellular DNA release. The ability of the dendrons to effectively release DNA was therefore investigated using a heparin sulfate displacement assay. Heparin sulfate is an anionic polymer, which can compete with DNA for binding to the cationic dendrons. Thus, the amount of heparin sulfate required to fully displace the DNA from the vector is a good indicator of how effectively the vector can release the DNA from its complex intracellularly. The experimental heparin sulfate competition assays were paralleled by atomistic molecular dynamics simulations Fig. (**25**) of direct binding ΔG_{bind} of each dendron micelle and a chain of heparin sulfate. As shown in (Table **8**), MM/PBSA ranked the affinity of the different dednon micelles toward heparin sulfate in the following order: Chol-G1 > Chol-G2 > C_{22}-G2 > C16-G2 > C_{12}-G2, in agreement with the affinities exhibited by these self-assemblies for DNA.

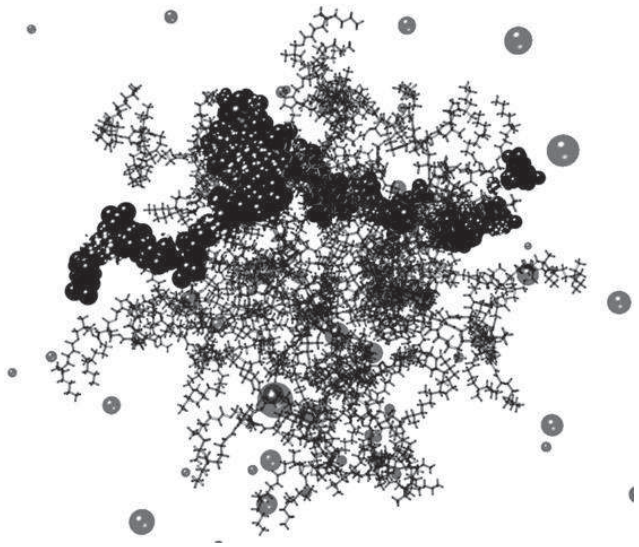

Fig. (25). Atomistic molecular dynamics simulation snapshot of the $Chol_2$-G2 micelle in complex with a fragment of heparin sulfate. The dendrons in the micelle are shown as gray sticks, while the heparin fragment is in black CPK representation. Cl^- and Na^+ ions are shown as big and small gray spheres, respectively. Water is not shown for clarity. Adapted from [54], with permission of the ACS.

More enlightening information is however obtained by considering the last column in (Table **8**) presenting the difference in binding affinity of each dendron micelle toward heparin sulfate and DNA, respectively. Since here $\Delta\Delta G_{bind}$ is defined as: $\Delta\Delta G_{bind} = \Delta G_{bind}$(heparin sulfate) - ΔG_{bind}(DNA), the more positive the value

Table 8. Free Energy of Binding ΔG_{bind} (kcal/mol) the Between Hydrophobically Modified Dendron Micelles and Heparin Sulfate. $\Delta\Delta G_{bind}$ = ΔG_{bind}(Heparin Sulfate) - ΔG_{bind}(DNA) (See Text for Mode Details). Adapted from [54], With Permission of the ACS

Compound	ΔG_{bind}	$\Delta\Delta G_{bind}$
C_{12}-G2	-12.0 ± 0.7	4.8 ± 1.5
C_{16}-G2	-12.2 ± 1.1	10.2 ± 2
C_{22}-G2	-22.4 ± 1.9	11.4 ± 3.4
Chol-G2	-67.6 ± 1.5	3.6 ± 2.8
$Chol_2$-G2	-103.9 ± 2.6	15.3 ± 4.0

of $\Delta\Delta G_{bind}$ for a given dendron micelle, the higher the affinity of that micelle toward DNA rather than to heparin sulfate. The data indicate that compound Chol2-G2 binds DNA much more effectively than heparin. This modeling study therefore verifies the experimentalresults provided by gel electrophoresis, in which Chol-G2 was best able to release the DNA and transfection studies in which Chol-G2 was the most e ff ective delivery vehicle. This provides further support to the concept that, although beneficial for complexation, compaction, protection transport, and cellular entry, if DNA binding is too tight in comparison with other anionic heparin is much more competitive with DNA species it is detrimental to the fundamental step of DNA release inside the target cell.

We propose that the better relative ability of Chol-G2 to bind heparin and release DNA may be a consequence of the higher surface charge density of Chol-G2 being better matched to the very high anionic surface charge density of heparin. We therefore reason that the cationic charge density of the self-assembled nanostructures may play an important role in enabling heparin-mediated DNA release. This would also explain why PEI, which has very high charge density, achieves such e ff ective DNA release under these conditions.

Give Me a Break! (Or Simulations of Nanovector Degradation for DNA/RNA Enhanced Release)

The DNA "overbinding" dendrons discussed above were designed to incorporate ester groups into the branched framework, providing them with the capacity to degrade under biological conditions of pH. It had been our intention that over biologically relevant time scales dendron degradation would occur, turning a multivalent ligand array into smaller units which were not capable of such effective DNA binding. We hoped that this would actually facilitate intracellular DNA release, helping overcome this DNA tight-binding barrier to gene transfection. We therefore designed an electrospray mass spectrometric (ES-MS) assay to probe the pathways of dendron degradation which were actually taking place. In general terms, all of the dendrons degraded with none of the initial dendron (100 μM) remaining after a period of 6/10 h — a transfection relevant time scale. At first sight, therefore, the MS assay would indicate that dendron degradation should occur under cellular conditions and encourage DNA release. However, we also found that dendron degradation does not occur at pH 5.0, relevant to the interior of endosomes. It is therefore possible that during trafficking into the cell degradation of the dendron is limited as it experiences the more acidic endosomal environment and that this is responsible for the poor DNA release and transfection profile.

To confirm that dendron degradation should, in principle, lead to DNA release, we performed further atomistic MD simulations starting from each dendron micelle in complex with a small fragment of ds-DNA. For this study, we detached surface ligands from the dendron by *in silico* degradation, and monitored the thermodynamics of binding by MM/PBSA calculations. The modeling is represented graphically in Fig. (**26**), which illustrates how our micelles lose their ability to bind to DNA as surface ligands are detached in this manner.

(Table **9**) collects the quantitative binding data which demonstrate that, as expected, the degraded products are less able to bind DNA than the intact dendrons when assembled into micellar form. Interestingly, the loss of DNA binding is more marked for Chol-G2 than for $Chol_2$-G2. For Chol-G2, when half of the ligands have been lost (i.e., degradation of one of the ester bonds as evidenced by mass spectrometry), the binding strength for DNA has dropped by ca. 70%. However, for $Chol_2$-G2, loss of half the binding ligands only leads to a decrease in binding affinity of 58%. Only on further degradation does the free energy of DNA binding for $Chol_2$-G2 drop significantly below 50 kcal/mol.

We suggested that the two hydrophobic cholesterol units in $Chol_2$-G2 are better able to maintain the self-assembled nanostructure during degradation, enabling the maintenance of a higher micellar surface positive charge density and allowing the micelles to hold onto DNA more effectively. These modeling observations would imply that if intracellular degradation is indeed occurring then Chol-G2 would be the better dendron for achieving rapid DNA release, in agreement with our experimental observations of gene delivery.

CONCLUSIONS

The extensive series of examples illustrated and discussed above - taken from our own experience in the field - emphasize the role and potentiality of multiscale molecular modeling in the pre- and post-development of nanodevices for gene delivery. Accurate and reliable molecular modeling can be performed more easily than experiments. *In silico* evaluation can take into account the molecular specificity of the problem and dramatically reduce the time and cost required to formulate a new device and therapeutic intervention, and eventually translate it into the clinical setting. In nanomedicine, the need for accurate multiscale molecular modeling is even more pressing. Despite its rapid growth and extraordinary potential, the field is still in its infancy, is highly interdisciplinary, and aims at solving problems of extraordinary and unprecedented complexity. With such a scenario, multiscale molecular modeling could dictate the success of nanomedicine and make the difference between several years of unfruitful research and the development of new, revolutionary therapeutic strategies readily available to the public.

CONFLICT OF INTEREST

The author(s) confirm that this article content has no conflicts of interest.

ACKNOWLEDGEMENTS

This wonderful experience in the multiscale molecular modeling of dendrimers and dendrons for gene therapy benefitted from a series of exciting and inspiring collaborations. The concrete chance

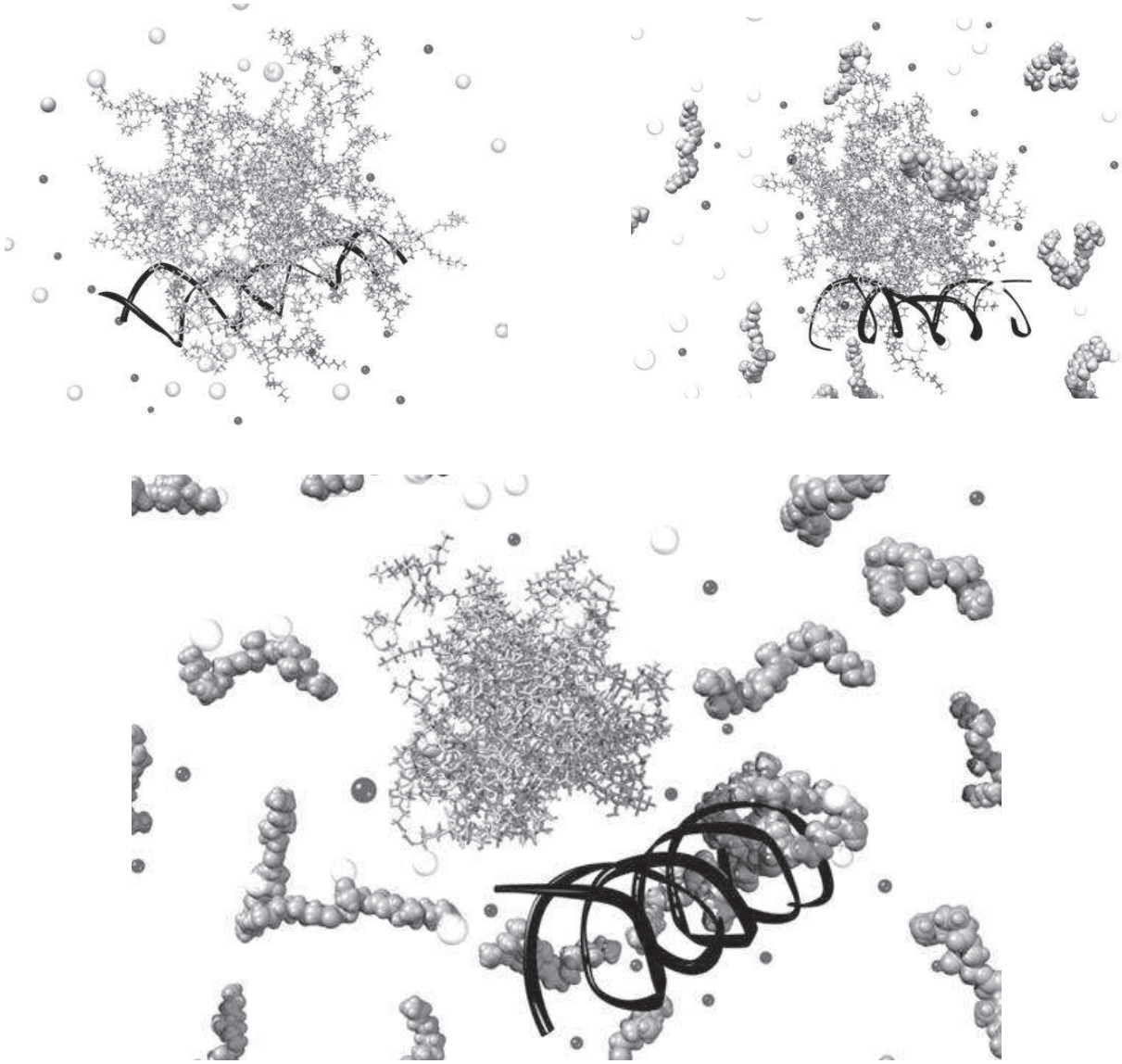

Fig. (26). Snapshots of the molecular dynamics simulations of the degradation of the Chol-G2 micelle in complex with a short fragment of ds-DNA. (Top left panel) intact Chol-G2 micelle binding DNA. (Top right panel) Chol-G2 micelle with half of the surface ligands detached. (Bottom panel) Chol-G2 micelle with all of the surface ligands detached.

Table 9. Free Energy of Binding ΔG_{bind} (kcal/mol) and Normalized Free Energy of Binding Per Charge on the Micelle $\Delta G_{bind}/N$ (kcal/mol) for DNA Binding of the Hydrophobically Modified Dendron Micelles With Sequential Ligand Detachment. Adapted from [54], With Permission of the ACS

Compound	Number of Ligands	ΔG_{bind}	$\Delta G_{bind}/N$
Chol-G2	4	-71.2 ± 2.4	-0.56 ± 0.02
	3	-47.7 ± 1.3	-0.50 ± 0.01
	2	-21.1 ± 1.1	-0.33 ± 0.02
	1	-10.0 ± 0.4	-0.31 ± 0.01
	0	-1.3 ± 0.4	-
$Chol_2$-G2	4	-119.2 ± 3.1	-0.68 ± 0.02
	3	-82.6 ± 2.2	-0.63 ± 0.02
	2	-49.7 ± 1.6	-0.56 ± 0.02
	1	-14.0 ± 0.3	-0.32 ± 0.02
	0	-1.8 ± 0.1	-

for these collaborations originated under the framework of the Cost Action TD 0802 "Dendrimers in Biomedical Applications", chaired by Prof. Barbara Klajnert, to which all authors are very much indebted. Financial support from the associated projects "DENANORNA " (International ERA-Net EURONANOMED grant), "DDOS" (ESTECO grant), the HPC-Europa 2 Project (CINECA Supercomputing Center grant in the Eu 7th Framework Program), and "MONALISA" (Iscra supercomputing grant) is gratefully acknowledged. The stripe of the B.C. comic is dedicated to the memory of its genius creator, Johnny Hart.

REFERENCES

[1] a) Watts, J.K.; Corey, D.R. Silencing disease genes in the laboratory and the clinic. *J. Pathol.,* **2012**, *226*(2), 365-379; b) Both, G.; Alexander, I.; Fletcher,S.; Nicolson, T.J.; Rasko, J.E.; Wilton, S.D.; Symonds, G. Gene therapy: therapeutic applications and relevance to pathology. *Pathology*, **2011**, *43*(6), 642-656; c) Gambari.; R.; Fabbri, E.; Borgatti, M.; Lampronti, I.; Finotti, A.; Brognara, E.; Bianchi, N.; Manicardi, A.; Marchelli, R.; Corradini, R. Targeting microRNAs involved in human diseases: a novel approach for modification of gene expression and drug development. *Biochem. Pharmacol*., **2011**, *82*(10), 1416-1429; d) G.C. Shukla; F. Haque; Y. Tor; L.M. Wilhelmsson; J.J. Toulmé; H. Isambert; P. Guo; J.J. Rossi; S. A. Tenenbaum; B.A. Shapiro. A boost for the emerging field of RNA nanotechnology. *ACS Nano*, **2011**, 5(5), 3405-3418., and references therein.

[2] Ruenraroengsak, P.; Cook, J.M.; Florence, A.T. Nanosystem drug targeting: Facing up complex realities. *J. Control. Rel*ease, **2010**, 141(3), 265-276.

[3] Reischl, D.; Zimmer. A. Drug delivery of siRNA therapeutics: potentials and limits of nanosystems. *Nanomedicine*: *Nanotech. Biol. Med*., **2009**, *5*(1), 8-20.

[4] Juliano, R.; Alam, R.; Dixit, V.; Kang, H. Mechanisms and strategies for effective delivery of antisense and siRNA oligonucleotides. *Nucl. Acid Res*., **2008**, *36*(12), 4158-4171.

[5] a) Behr, J.P. Synthetic gene transfer vectors II: back to the future. *Acc. Chem. Res*., Article ASAP, Publication Date (Web): February 6, 2012, DOI: 10.1021/ar200213g; b) Mintzer, M.A.; Simanek, E.E. Nonviral vectors for gene delivery. *Chem. Rev*., **2009**, *109*(2), 259-302; c) Jeong, J.H.; Kim, S.W.; Park, T.G. molecular design of functional polymers for gene therapy. *Progr. Polym. Sci*. **2007**, *32*(11), 1239-1274.

[6] a) Wang, M.; Thanou, M. Targeting nanoparticles to cancer. *Pharm. Res*., **2010**, *62*(1), 90-99; b) Mishra, B.; Patel, B.B.; Tiwari, S. Colloidal nanocarriers: a review on formulation technology, types, and applications toward drug delivery. *Nanomedicine*: *Nanotech. Biol. Med*., **2010**, *6*(1), 9-24; c) de Martinprey, H.; Vauthier, C.; Malvy, C.; Couvreur, P. Polymer nanocarriers for the delivery of small fragments of nucleic acids: oligonucleotides and siRNA. *Eur. J. Pharm. Biopharm*., **2009**, *71*(3), 490-504; d) Christian, D.A.; Cai, S.; Bowen, D.M.; Kim, Y.; Pajerowski, D.; Discher, D.E. Polymersome carriers: from self-assembly to siRNA and protein therapeutics. *Eur. J. Pharm. Biopharm*., **2009**, *71*(3), 463-467; e) Ferrari, M. Nanovector therapeutics. *Curr. Opin. Chem. Biol*., **2005**, *9*(4), 343-346; f) Ferrari, M. Cancer nanotechnology: opportunities and challenges. *Nat. Rev. Cancer*, **2005**, *5*(3), 161-71.

[7] a) Sakamoto, J.H.; van de Ven, A.L.; Godin, B.; Blanco, E.; Serda, R.E.; Grattoni, A., *et al.* Enabling individualized therapy through nanotechnology. *Pharmacol. Res*., **2010**, *62*(2), 57-89; b) Singh, R.; Lillard, J.W. Nanoparticle-based targeted drug delivery. *Exp. Mol. Pathol*., **2009**, *86*(3), 215-223.

[8] Posocco, P.; Fermeglia, M.; Pricl, S. Morphology prediction of block copolymers for drug delivery by mesoscale simulations. *J. Mater. Chem*., **2010**, *20*, 7742-7753.

[9] a) Tomalia, D.A. A new class of polymers: starburst-dendritic macromolecules. *Polym. J*., **1985**, *17*, 117-132.

[10] Lee, C.C.; MacKay, J.A.; Frechet, J.M.; Szoka, F.C. Designing dendrimers for biological applications. *Nat. Biotechnol*., **2005**, *23*(12), 1517-1526.

[11] Tomalia, D.A.; Naylor, A.M.; Goddard, W.A. III. Starburst dendrimers: molecular-level control of size, shape, surface shemistry, topology, and flexibility from atoms to macroscopic matter. *Angew. Chem. Int. Ed. Engl*., **1990**, *29*(2), 138-175.

[12] Svenson, S. Dendrimers as versatile platform in drug delivery applications. *Eur. J. Pharm. Biopharm*., **2009**, *71*(3), 445-462.

[13] Liu, M.; Frechet, J.M. designing dendrimers for drug delivery. *Pharm. Sci. Technol. Today*, **1999**; *2*(10), 393-401.

[14] a) Cheng, Y.; Zhao, L.; Li, Y.; Xu, T. Design of biocompatible dendrimers for cancer diagnosis and therapy: current status and future perspectives. *Chem. Soc. Rev*., **2011**, *40*, 2673-2703; b) Medina, S.H.; El-Sayed, M.E.H. Dendrimers as carriers for delivery of chemotherapeutic agents. *Chem. Rev*., **2009**, *109*(7), 3141-3157; c) Tekade R.K.; Kumar, P.V.; Jain, N.K. Dendrimers in oncology: an expanding horizon. *Chem. Rev*., **2009**, *109*(1), 49-87; d) Rolland, O.; Turrin, C.O.; Caminade, A.M.; Majoral, J.P. Dendrimers and nanomedicine: multivalency in action. *New J. Chem*. **2009**, *33*, 1809-1824.

[15] National science and Technology Council Committee on Technology. The National Nanotechnology Initiative: research and development leading to a revolution in technology and industry. Washington DC: Office of Science and Technology Policy, **2005**.

[16] Koo, O.; Rubinstein, I.; Onyuksel, H. Role of nanotechnology in target drug delivery and imaging: a concise review. *Nanomedicine: Nanotech. Biol. Med*., **2005**, *1*(3), 193-212.

[17] a) Toth, R.; Santese, F.; Pereira, S.P.; Nieto, D.R.; Pricl, S.; Fermeglia, M.; Posocco, P. Size and shape matter! A multiscale molecular simulation approach to polymer nanocomposites. *J. Mater. Chem*., First published on the web: 07 Feb 2012, doi: 10.1039/C2JM15763B; b) Posocco, P.; Fermeglia, M.; Pricl, S. Morphology prediction of block copolymers for drug delivery by mesoscale simulations. *J. Mater. Chem*., **2010**, *20*, 7742-7753; c) Scocchi, G.; Posocco, P.; Handgraaf, J.-W.; Fraaije, J.G.; Fermeglia, M.; Pricl, S. A complete multiscale modeling approach for polymer-clay nanocomposites. *Chem. Eur. J*., **2009**, *15*(31), 7586-7592; d) Toth, R.; Voorn, D.-J; Handgraaf, J.-W.; Fraaije, J.G.E.M.; Fermeglia, M.; Pricl, S.; Posocco, P. *Macromolecules*, **2009**, *42*(21), 8260–8270; e) Fermeglia, M.; Pricl, S. *Computers & Chem. Eng*., **2009**, *33*, 1701-1710 and references therein.

[18] a) Hoogerbrugge, P.J.; Koelman, J.M.V.A. Simulating microscopic hydrodynamic phenomena with dissipative particle dynamics. *Europhys. Lett*., **1992**, *19*(3), 155-160; b) Español, P.; Warren, P.B. Statistical mechanics of dissipative particle dynamics. *Europhys. Lett*., **1995**, *30*(4), 191-196; c) Groot, R.D.; Warren, P.B. Dissipative particle dynamics: bridging the gap between atomistic and mesoscopic simulation. *J. Chem. Phys.*, **1997**, *107*(11), 4423-4435.

[19] Tang, M.X.; Redemann, C.T.; Szoka, F.C. *In vitro* gene delivery by degraded polyamidoamine dendrimers. *Bioconjugate Chem*. **1996**, *7*(6), 703-714.

[20] Sonawane, N.D.; Szoka, F.C., Verkman, A.S. Chloride accumulation and swelling in endosomes enhances DNA transfer by polyamine-DNA polyplexes. *J. Biol. Chem*., **2003**, *278*(45), 44826-44831.

[21] a) Liu, X.X.; Rocchi, P.; Qu, F.; Zheng, S.; Liang, Z.C.; Gleave, M.; Iovanna, J.; Peng, L. PAMAM dendrimers mediate siRNA delivery to target Hsp27 and produce potent antiproliferative effects on prostate cancer cells. *ChemMedChem*, **2009**, *4*(8), 1302-1310; b) Shen, X.C.; Zhou, J.; Liu, X.X.; Wu, J.; Qu, F.; Zhang, Z.L.; Pang, D.W.; Quelever, G.; Zhang, C.C.; Peng, L. Importance of size-to-charge ratio in the construction of stable and uniform nanoscale RNA/dendrimer complexes. *Org. Biomol. Chem*., *2007*, *5*, 3674-3681; c) Zhou, J.; Wu, J.; Hafdi, N.; Behr, J.P.; Erbacher, P., Peng, L. PAMAM dendrimers for efficient siRNA delivery and potent gene silencing. *Chem. Commun*., **2006**, 2362-2364; d) Wu, J.; Zhou, J.; Qu, F.; Bao, P.; Zhang, Y.; Peng, L. Polycationic dendrimers interact with RNA molecules: polyamine dendrimers inhibit the catalytic of *Candida* ribozymes. *Chem. Commun*., **2005**, 313-315.

[22] a) Posocco, P.; Ferrone, M.; Fermeglia, M.; Pricl, S. Binding at the core. Computational study of structural and ligand binding properties of naphthiridine based dendrimers. *Macromolecules*, **2007**, *40*(6), 2257-2266; b) Metullio, L.; Ferrone, M.; Coslanich, A.; Fuchs, S.; Fermeglia, M.; Paneni, M.S.; Pricl, S. Polyamidoamine (yet not PAMAM) dendrimers as bioinspired materials for drug delivery: structure-activity relationships by molecular simulations. *Biomacromolecules*, **2004**, *5*(8), 1371-1378; c) Pricl, S.; Fermeglia, M.; Ferrone, M.; Asquini, A. Scaling properties in the molecular structure of three-dimensional, nanosized phenylene-based dendrimers as studied by atomistic molecular dynamics simulations. *Carbon*, **2003**, *41*(12), 2269-2283; d) Fermeglia, M.; Ferrone, M.; Pricl, S. Computer-aided simulation of a dendrimer with a protoporphyrinic core as potential, novel hemoprotein mimic. *Bioorg. Med. Chem*., **2002**, *10*(12), 2471-2478; e) Tomalia, D.A.; Uppuluri, S.; Swanson, D.R.; Li, J. Dendrimers as reactive modules for the synthesis of new structure-controlled, higher-complexity megamers. *Pure Appl. Chem*., **2000**, *72*(12), 2343-2358.

[23] Liu, X.X.; Wu, J.; Yammine, M.; Zhou, J.; Posocco, P.; Viel, S.; Liu, C.; Ziarelli, F.; Fermeglia, M.; Pricl, S.; Victorero, G.; Nguyen, C.; Erbacher, P.; Behr, J.P.; Peng, L. Structurally flexible triethanolamine core PAMAM dendrimers are effective nanovectors for DNA transfection *in vitro* and *in vivo* to the mouse thymus. *Bioconjug. Chem*., **2011**, *22*(12), 2461-2473.

[24] Karatasos, K.; Posocco, P.; Laurini, E.; Pricl, S. Poly(amidoamine)-based dendrimer/siRNA complexation studied by computer simulations: effects of pH and generation on dendrimer structure and siRNA binding. *Macromol Biosci*., **2012**, *12*(2), 225-240.

[25] Huissmann, S.; Likos, C.N.; Blaak, R. Conformations of high-generation dendritic polyelectrolytes. *J. Mater. Chem*., **2010**, *20*, 10486-10494; b) Karatasos, K.; Adolf, D.B.; Davies, G.R. Statics and dynamics of model dendrimers as studied by molecular dynamics simulations. *J. Chem. Phys*., **2001**, *115*, 5310-5318.

[26] Fant, K.; Esbjorner, E.K.; Lincoln, P.; Norden, B. DNA condensation by PAMAM dendrimers: self-assembly characteristics and effect on transcription. *Biochemistry*, **2008**, *47*(6), 1732-1740.

[27] Bielinska, A.U.; Kukowska-Latallo, J.F.; Baker, J.J. The interaction of plasmid DNA with polyamidoamine dendrimers: mechanism of complex formation and analysis of alterations induced in nuclease sensitivity and transcriptional activity of the complexed DNA. *Biochim. Biophys. Acta*, **1997**, *1353*(2), 180-190.

[28] Gary, D.; Pury, N.; Won, Y. Polymer-based siRNA delivery: perspectives on the fundamental and phenomenological distinctions from polymer-based DNA delivery, *J. Control. Release*, **2007**, *121*(1-2), 64-73.

[29] Bolcato-Bellemin, A. L.; Bonnet, M. E.; Creusat, G.; Erbacher, P.; Behr, J. P.

Sticky overhangs enhance siRNA-mediated gene silencing. *Proc. Natl. Acad. Sci. U.S.A*., **2007**, *104*(41), 16050-16055.

[30] Liu, X.; Liu, C.; Laurini, E.; Posocco, P.; Pricl, S.; Qu, F.; Rocchi, P.; Peng, L. Efficient delivery of sticky siRNA and potent gene silencing in a prostate cancer model using a generation 5 triethanolamine-core PAMAM dendrimer. *Mol. Pharm*., Article ASAP, Publication Date (Web): December 30, 2011, doi:10.1021/mp2006104.

[31] a) Gomez-Casado, A.; Dam, H.H.; Yilmaz, M.D.; Florea, S.; Jonkheijm; P.; Huskens, J. Probing multivalent interactions in a synthetic host-guest complex by dynamic force spectroscopy. *J. Am. Chem. Soc*., **2011**, *133*(28), 10849-10857; b) Kane, R.S. Thermodynamics of Multivalent Interactions: Influence of the linker. *Langmuir*, **2010**, *26*(11), 8636-8640; c) Free energy balance predicated dendrimer binding multivalency at molecular printboards. *Langmuir*, **2007**, *23*(16), 8441-8451; d) Badjic, J.D.; Nelson, A.; Cantrill, S.J.; Turnbull, W.B.; Stoddard, J.F. Multivalency and Cooperativity in Supramolecular Chemistry. *Acc. Chem. Res*. **2005**, *38*(9), 723-732; e) Huskens, J.; mulder, A.; Auletta, T.; Nijhuis, C.A.; Ludden, M.J.W.; Reinhoudt, D.N. A model for describing the thermodynamics of multivalent host-guest interactions at interfaces. *J. Am. Chem. Soc*., **2004**, *126*(21), 6784-6797; f) Christensen, T.; Gooden, D.M.; Kung, J.E.; Toone, E.J. Additivity and the physical basis of multivalency effects: a thermodynamic investigation of the Calcium EDTA interaction. *J. Am. Chem. Soc*., **2003**, *125*(24), 7357-7366; g) Kitov, P.I.; Bundle, D.R. On the nature of the multivalence effect: a thermodynamic model. *J. Am. Chem. Soc*., **2003**, *125*(52), 16271-16284.

[32] Rosen, B.M.; Wilson, C.J.; Wilson, D.A.; Peterca, M.; Imam, M.R.; Percec, V. Dendron-mediated self-Assembly, disassembly, and self-organization of complex systems. *Chem. Rev*., **2009**, *109*(11), 6275-6540.

[33] Smith, D.K.; Hirst, A.R.; Love, C.S.; Hardy, J.G.; Brignell, S.V.; Huang, B. Self-assembly using dendritic building blocks – towards controllable nanomaterials. *Prog. Polym. Sci*., **2005**, *30*(3-4), 220-293.

[34] a) Hamley, J.W. nanotechnology with soft materials. *Angew. Chem. Int. Ed*., **2003**, *42*(15), 1692-1712; b) Whitesides, G.M.; Grzybowski, B. Self-assembly at all scales. *Science*, **2002**, *295*(5564), 2418-2421.

[35] a) Steed, J.W.; Atwood, J.L. *Supramolecular Chemistry*. Wiley & Sons: Chichester, **2000**; b) Beer, P.D.; Gale, P.A., Smith, D.K. Supramolecular Chemistry. Oxford University Press: Oxford, **1999**.

[36] a) Smith, D.K. Recent developments in dendrimer chemistry. *Tetrahedron*, **2003**, *59*(22), 3797-3798; b) Smith, D.K.; Diederich, F. Supramolecular dendrimer chemistry: a journey through the branched architecture. *Top. Curr. Chem*., **2000**, *210*, 183-227.

[37] Jones, S.P.; Gabrielson, N.P.; Pack, D.W.; Smith, D.K. Synergistic effects in gene delivery - a structure-activity approach to the optimisation of hybrid dendritic-lipidic transfection agents. *Chem. Commun*., **2008**, 4700–4702.

[38] Posocco, P.; Pricl, S.; Jones, S.P.; Barnard, A.; Smith, D.K. Less is more - – multiscale modeling of self-assembling multivalency and its impact on DNA binding and gene delivery. *Chem. Sci*., **2010**, *1*, 393-404.

[39] Jones, S.P.; Pavan, G.M.; Danani, A.; Pricl, S.; Smith, D.K. Quantifying the effect of surface ligands on dendron-DNA interactions: insights into multivalency through a combined experimental and theoretical approach. *Chem. Eur. J*., **2010**, *16*(15), 4519-4532.

[40] Pavan, G.M.; Danani, A.; Pricl, S.; Smith, D.K. Modeling the multivalent recognition between dendritic molecules and DNA: understanding how ligand "sacrifice" and screening can enhance binding. J. Am. Chem. Soc., 2009, 131(28), 9686-9694.

[41] (a) Israelachvili, J.N.; Mitchell, D.J.; Ninham, B.W. Theory of self-assembly of lipid bilayers and vesicles. *Biochim. Biophys. Acta, Biomembr*., **1977**, *470*(2), 185-201; b) Israelachvili, J.N.; Mitchell, D.J.; Ninham, B.W. Theory of self-assembly of hydrocarbon amphiphiles into micelles and bilayers. *J. Chem. Soc., Faraday Trans. II*, **1976**, 72(2), 1525-1568.

[42] Jones, S.P.; Gabrielson, N.P.; Wong, C.H.; Chow, H.F.; Pack, D.W.; Posocco, P.; Fermeglia, M.; Pricl, S.; Smith, D.K. Hydrophobically modified dendrons: developing structure-activity relationships for DNA binding and gene transfection. *Mol Pharm*., **2011**, *8*(2), 416-429.

[43] Abdelhady, H.G.; Allen, S.; Davies, M.C.; Roberts, C.J.; Tendler, S.J.B.; Williams, P.M. Direct real-time molecular scale visualization of the degradation of condensed DNA complexed exposed to DNase I. *Nucleic Acid Res*., **2003**, *31*(14), 4001-4005.

[44] a) Dorigo, B.; Schalch, T.; Kulangara, A.; Duda, S.; Schroeder, R.; Richmond, T.J. Nucleosome arrays reveal the two-start organization of the chromatin fibers. *Science*, **2004**, *306*(5701), 1571-1573; b) Olins, A.L.; Olins, D.E. Spheroid chromatin units. *Science*, **1974**, *183*(4122), 330-332.

[45] Marenduzzo, D.; Finan, K.; Cook, P.R. The depletion attraction: an underappreciated force driving cellular organization. *J. Cell. Biol*., **2006**, *175*(5), 681-686.

[46] Manning, G.S. Limiting laws and counterion condensation in polyelectrolyte solution. *J. Chem. Phys*., **1969**, *51*(3), 924-933.

[47] (a) May, S., Ben-Shaul, A. Modeling of cationic lipid-DNA complexes. *Curr. Med. Chem*., **2004**, 11(2), 151-167; b) Harries, D.; May, S.; Gelbart, W.M.; Ben-Shaul, A. Structure, stability, and thermodynamics of lamellar DNA-lipid complexes. *Biophys. J*., **1998**, *75*(1), 159-173; c) Bruinsma, R. Electrostatics of DNA cationic lipid complexes: isoelectric instability. *Eur. Phys. J*., **1998**, *B4*, 75-78.

[48] Tanford, C. The hydrophobic effect: formation of micelles and biological membranes, 2nd ed. Krieger Publishing Co., Malabar, FL, **1991**.

[49] (a) Patrickios, C.S. Micellization model for multivalent ionic surfactants. *J. Phys. Chem*., **1995**, *99*(48), 17437-17441; (b) Nagarajan, R. Molecular packing parameter and surfactant self-assembly: the neglected role of the surfactant tail. *Langmuir*, **2002**, *18*(1), 31-38.

[50] Tomas, S.; Milanesi, L. Hydrophobically self-assembled nanoparticles as molecular receptors in water. *J. Am. Chem. Soc*., **2009**, *131*(18), 6618-6623.

[51] a) Sella, E.; Shabat, D. *Chem. Commun*., **2008**, 5701-5703; b) Sagi, A.; Segal, E.; Satchi-Fainaro, R.; Shabat, D. *Bioorg. Med. Chem*., **2007**, *15*(11), 3720-3727; c) Perry, R.; Amir, R.J.; Shabat, D. *New J. Chem*., **2007**, *31*, 1307-1312; d). Kevwitch, R.M.; McGrath, D.V. *New J. Chem*., **2007**, *31*, 1332-1336, and references therein.

[52] Kostiainen, M.A.; Smith, D.K.; Ikkala, O. *Angew. Chem. Int. Ed*., **2007**, *46*, 7600-7604.

[53] Welsh, D.J.; Jones, S.P.; Smith, D.K. *Angew. Chem. Int. Ed*., **2009**, *48*, 4047-4050.

[54] Barnard, A.; Posocco, P.; Pricl, S.; Calderon, M.; Haag, R.; Hwang, M.E.; Shum, V.W.; Pack, D.W.; Smith, D.K. Degradable self-assembling dendrons for gene delivery: experimental and theoretical insights into the barriers to cellular uptake. *J. Am. Chem. Soc*., **2011**, *133*(50),20288-20300.

Received: February 20, 2012 **Revised: May 28, 2012** **Accepted: June 21, 2012**